AMERICAN SOCIETY FOR MICROBIOLOGY | Journal of Virology®



# Pivotal Role of Receptor-Interacting Protein Kinase 1 and Mixed Lineage Kinase Domain-Like in Neuronal Cell Death Induced by the Human Neuroinvasive Coronavirus OC43

**Mathieu Meessen-Pinard, Alain Le Coupanec, Marc Desforges, Pierre J. Talbot**

Laboratory of Neuroimmunovirology, INRS-Institut Armand-Frappier, Université du Québec, Laval, Québec, Canada

**ABSTRACT** Human coronaviruses (HCoV) are respiratory pathogens with neuroinvasive, neurotropic, and neurovirulent properties, highlighting the importance of studying the potential implication of these viruses in neurological diseases. The OC43 strain (HCoV-OC43) was reported to induce neuronal cell death, which may participate in neuropathogenesis. Here, we show that HCoV-OC43 harboring two point mutations in the spike glycoprotein (rOC/$U_{s183–241}$) was more neurovirulent than the wild-type HCoV-OC43 (rOC/ATCC) in mice and induced more cell death in murine and human neuronal cells. To evaluate the role of regulated cell death (RCD) in HCoV-OC43-mediated neural pathogenesis, we determined if knockdown of Bax, a key regulator of apoptosis, or RIP1, a key regulator of necroptosis, altered the percentage of neuronal cell death following HCoV-OC43 infection. We found that Bax-dependent apoptosis did not play a significant role in RCD following infection, as inhibition of Bax expression mediated by RNA interference did not confer cellular protection against the cell death process. On the other hand, we demonstrated that RIP1 and MLKL were involved in neuronal cell death, as RIP1 knockdown and chemical inhibition of MLKL significantly increased cell survival after infection. Taken together, these results indicate that RIP1 and MLKL contribute to necroptotic cell death after HCoV-OC43 infection to limit viral replication. However, this RCD could lead to neuronal loss in the mouse CNS and accentuate the neuroinflammation process, reflecting the severity of neuropathogenesis.

**IMPORTANCE** Because they are naturally neuroinvasive and neurotropic, human coronaviruses are suspected to participate in the development of neurological diseases. Given that the strain OC43 is neurovirulent in mice and induces neuronal cell death, we explored the neuronal response to infection by characterizing the activation of RCD. Our results revealed that classical apoptosis associated with the Bax protein does not play a significant role in HCoV-OC43-induced neuronal cell death and that RIP1 and MLKL, two cellular proteins usually associated with necroptosis (an RCD back-up system when apoptosis is not adequately induced), both play a pivotal role in the process. As necroptosis disrupts cellular membranes and allows the release of damage-associated molecular patterns (DAMP) and possibly induces the production of proinflammatory cytokines, it may represent a proinflammatory cell death mechanism that contributes to excessive neuroinflammation and neurodegeneration and eventually to neurological disorders after a coronavirus infection.

**KEYWORDS** coronavirus, human coronavirus, human coronavirus OC43, regulated cell death, necroptosis, RIP

**Received** 29 July 2016 **Accepted** 12 October 2016

**Accepted manuscript posted online** 19 October 2016

**Citation** Meessen-Pinard M, Le Coupanec A, Desforges M, Talbot PJ. 2017. Pivotal role of receptor-interacting protein kinase 1 and mixed lineage kinase domain-like in neuronal cell death induced by the human neuroinvasive coronavirus OC43. J Virol 91:e01513-16. https://doi.org/10.1128/JVI.01513-16.

**Editor** Douglas S. Lyles, Wake Forest University



Address correspondence to Pierre J. Talbot, pierre.talbot@iaf.inrs.ca, or Marc Desforges, marc.desforges@iaf.inrs.ca.

Human coronaviruses (HCoV) are largely associated with the common cold, whereas the elderly, newborns, infants, and immunocompromised individuals are more susceptible to the development of severe lower respiratory infection, such as pneumonia or bronchitis (1). Over the years, evidence has accumulated to support the idea that HCoV can act as opportunistic pathogens that can be associated with other pathologies, including neurological disorders (2–6). Moreover, HCoV-OC43 has recently been detected in the brain of an immunodeficient child who died from fatal encephalitis (7).

Like its murine counterpart, mouse hepatitis virus (MHV), which is recognized to induce neurological disorders in mouse models (8, 9), we have previously demonstrated that the human coronavirus strain OC43 (HCoV-OC43) possesses neuroinvasive and neurotropic properties that allow the virus to invade, spread, and persist within the murine central nervous system (CNS), where neurons represent the main target during the acute phase of infection (10, 11). Furthermore, HCoV-OC43 is also naturally neuroinvasive in humans, as RNA was detected in human brain samples of patients suffering from neurological diseases, such as Alzheimer's, Parkinson's disease, and multiple sclerosis, and in controls (12). Furthermore, we have previously demonstrated that HCoV-OC43 has the capacity to induce neuronal cell death (11, 13) associated with the induction of the unfolded protein response (UPR) and endoplasmic reticulum (ER) stress, as well as degeneration of neurons (13–17). However, the exact underlying mechanism of neuronal cell death induced during HCoV-OC43 infection remains poorly understood, and its involvement in neuropathogenesis is still unclear.

Regulated cell death (RCD) represents a large homeostasis system that controls several aspects of cell life (18). One of these roles may be considered a defense mechanism against viral infection in order to control or limit propagation and protect the entire organism (19, 20). Different RCD pathways are now identified based on biochemical features in order to improve our understanding of cell response to stress (21). The most known and studied form of RCD is caspase-dependent apoptosis, characterized by extracellular stress signals sensed by receptors (extrinsic apoptosis) or intracellular stress (intrinsic apoptosis), which activates specific cellular factors, including caspase-8 and the proapoptotic Bax protein, which converge to trigger the activation of downstream effector caspases (22–24). More recently, necroptosis, another form of RCD, has gained attention, as this regulated necrosis independent of caspases can act to replace classical apoptosis pathways (25). Necroptosis often involves attachment of tumor necrosis factor alpha (TNF-$\alpha$) to its receptor (TNFR1) on the cell surface, which can induce a downstream death signal characterized by a core component composed of receptor-interacting protein kinase 1 (RIP1) and RIP3 interacting with each other (26). In the case where caspase-8 activity is somehow abrogated, RIP1 can interact with RIP3 and the complex is activated by phosphorylation (27–30). The RIP1-RIP3 complex then participates in the cell membrane disruption mediated by the phosphorylated form of mixed lineage kinase domain-like (MLKL) and ultimately in cell death (31–33).

In the present study, we sought to further investigate the underlying mechanisms of HCoV-OC43-induced neuronal cell death after infection by identifying cellular factors involved in the different pathways associated with RCD and their potential association with neuropathogenesis during a CNS infection. Overall, the global portrait suggests that Bax-dependent apoptosis is not significantly involved during infection of human neuronal cells by HCoV-OC43 but that necroptosis, which involves RIP1 and MLKL, seems to play a central role in the regulation of neuronal cell death in order to limit viral replication and propagation.

## RESULTS

**rOC/U$_{s183–241}$ is more neurovirulent than rOC/ATCC in mice despite similar production of infectious viral particles in the CNS.** We have previously shown that HCoV-OC43 infection leads to human neuronal cell death (13) and that a variant harboring two point mutations in the viral spike (S) glycoprotein (rOC/U$_{s183–241}$) showed a significant increase in virus-induced neuronal cell mortality compared to the

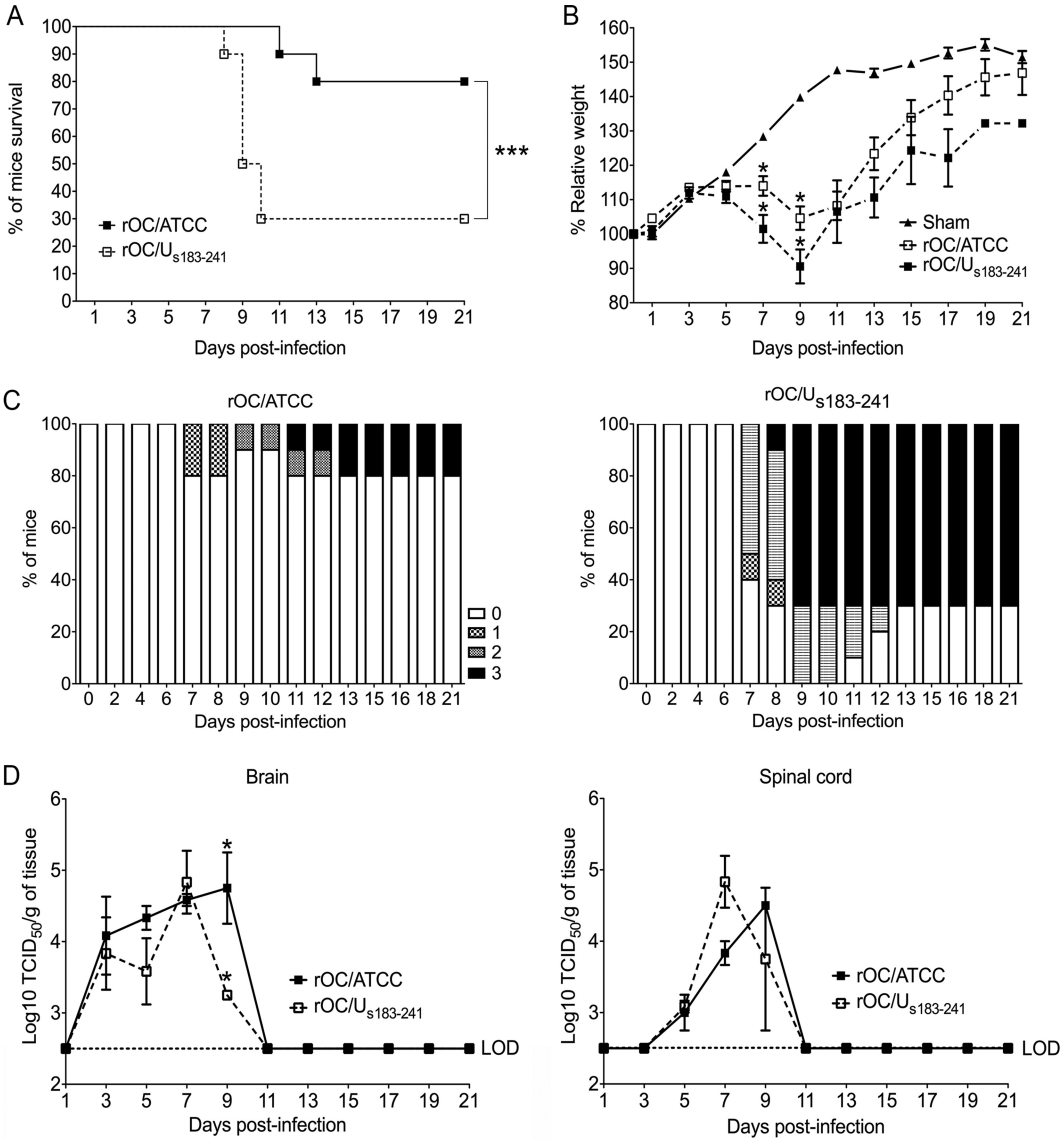


**FIG 1** rOC/$U_{s183–241}$ is more neurovirulent than rOC/ATCC in infected mice. Twenty-two-day-old BALB/c female mice received $10^{2.5}$ $TCID_{50}$/10 $\mu$l of rOC/ATCC or rOC/$U_{s183–241}$ or were inoculated with PBS by the i.c. route. (A) Survival curves of mice, in percentages, over a period of 22 days (dpi). (B) Weight variations were measured every 2 days during 22 days and expressed as percent variation compared to day 0. (C) Evaluation of clinical scores (percentage of mice at each level of the scale) of mice infected by rOC/ATCC (left) or rOC/$U_{s183–241}$ (right). (D) Production of infectious particles was measured in the brain (left) and spinal cord (right) of infected mice. LOD represents limit of detection. Results are representative of two independent experiments, and error bars represent standard deviations (SD). Statistical significance is indicated by asterisks: *, $P < 0.05$; ***, $P < 0.001$.

reference variant (rOC/ATCC) (14). Some other variants of HCoV-OC43 were shown to have different levels of neurovirulence in infected mice. However, the relationship between neuronal cell death and neurovirulence remains poorly understood. In order to evaluate the neurovirulence of HCoV-OC43, we compared 22-day-old BALB/c mice infected by the intracerebral (i.c.) route with the wild-type (wt; rOC/ATCC) or mutant (rOC/$U_{s183–241}$) virus, with the latter being known to increase cell death of the infected human neuronal cell line LA-N-5 (13). Neurovirulence of both viruses was monitored by survival curves, as already reported (15), but weight loss and clinical scores of neurological symptoms (34) were also evaluated, and all of these parameters indicated that the S mutant virus rOC/$U_{s183–241}$ was more neurovirulent than the wt virus rOC/ATCC (Fig. 1A to C). Although we observed multiple clinical signs related to encephalitis for both viral infections, as seen by social isolation, abnormal flexion of the four limbs,

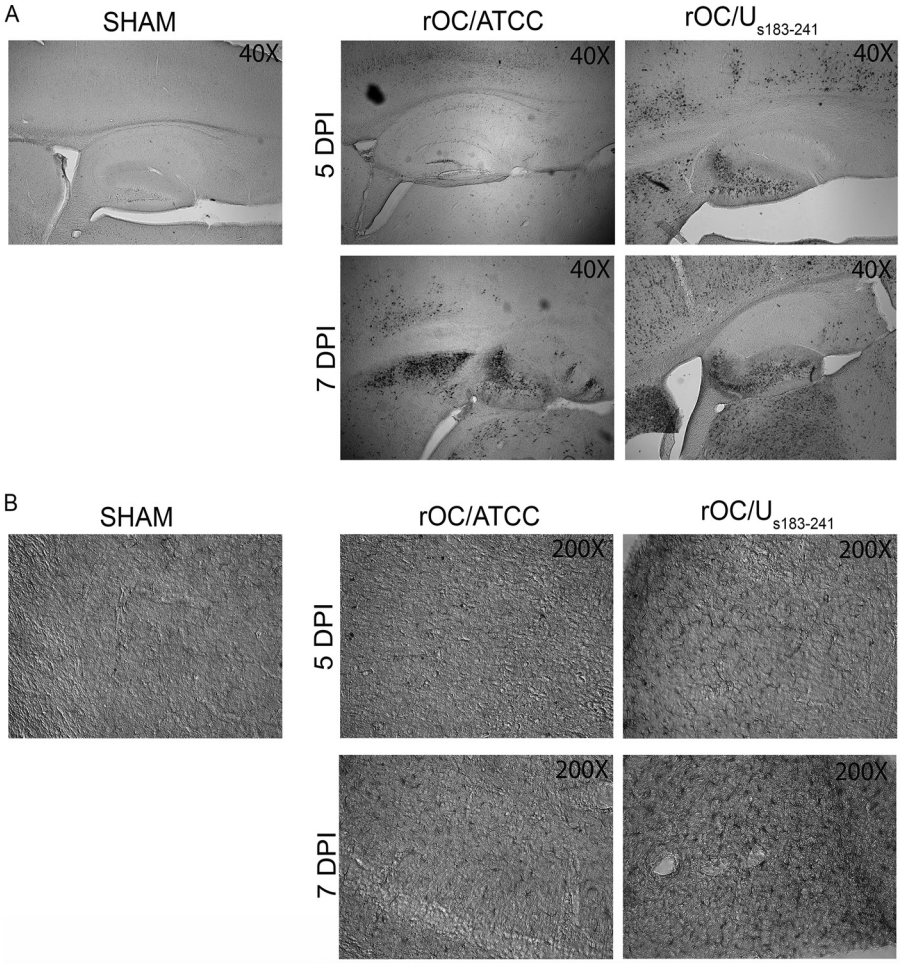


**FIG 2** rOC/$U_{s183–241}$ disseminates more rapidly in the brain and induces a stronger activation of astrocytes than rOC/ATCC in infected mice. Histological examination of hippocampus of 22-day-old BALB/c mice infected with $10^{2.5}$ $TCID_{50}$/10 $\mu$l of rOC/ATCC or rOC/$U_{s183–241}$ or inoculated with PBS. (A) Detection of viral antigen (N protein) at 5 and 7 dpi at a magnification of ×40. (B) Detection of glial fibrillary acidic protein (GFAP) in astrocytes (marker of astrogliosis) at 5 and 7 dpi at a magnification of ×200.

ruffled fur, and hunched back, most of the mice infected by the mutant virus presented four distinct levels of clinical scores more rapidly (Fig. 1C) and eventually a higher mortality rate than mice infected by the reference virus. To determine whether the difference in neurovirulence observed between rOC/$U_{s183–241}$ and rOC/ATCC was related to viral replication in the CNS, we measured infectious viral particles in brain and spinal cord every 2 days over a period of 22 days (Fig. 1D). Titers of infectious particles in the brain were the same for both viruses, although rOC/$U_{s183–241}$ could be cleared more rapidly than the wild-type virus, as observed at 9 days postinfection (dpi) (Fig. 1D, left). Similar to the brain, infection of the spinal cord by both viruses resulted in a similar production of viral particles; however, the mutant virus replicated more rapidly in the spinal cord (Fig. 1D, right). Altogether, these results indicate that rOC/$U_{s183–241}$ was more neurovirulent than the reference virus in mice infected after i.c. inoculation.

**Viral dissemination and astrocyte activation are more important following rOC/$U_{s183–241}$ infection than rOC/ATCC infection.** Hippocampus is one of the first regions where HCoV-OC43 spreads in the mouse CNS (17). Histological examination revealed that rOC/$U_{s183–241}$ reached this portion of the brain faster than rOC/ATCC, for which no antigens were observed before 7 dpi (Fig. 2A). The infection with either virus showed similar disseminated patterns in other regions of the brain, such as olfactory bulb and cortex (data not shown). As both viruses spread within the CNS, astrogliosis, considered a marker of inflammation, was also investigated and was detected in the

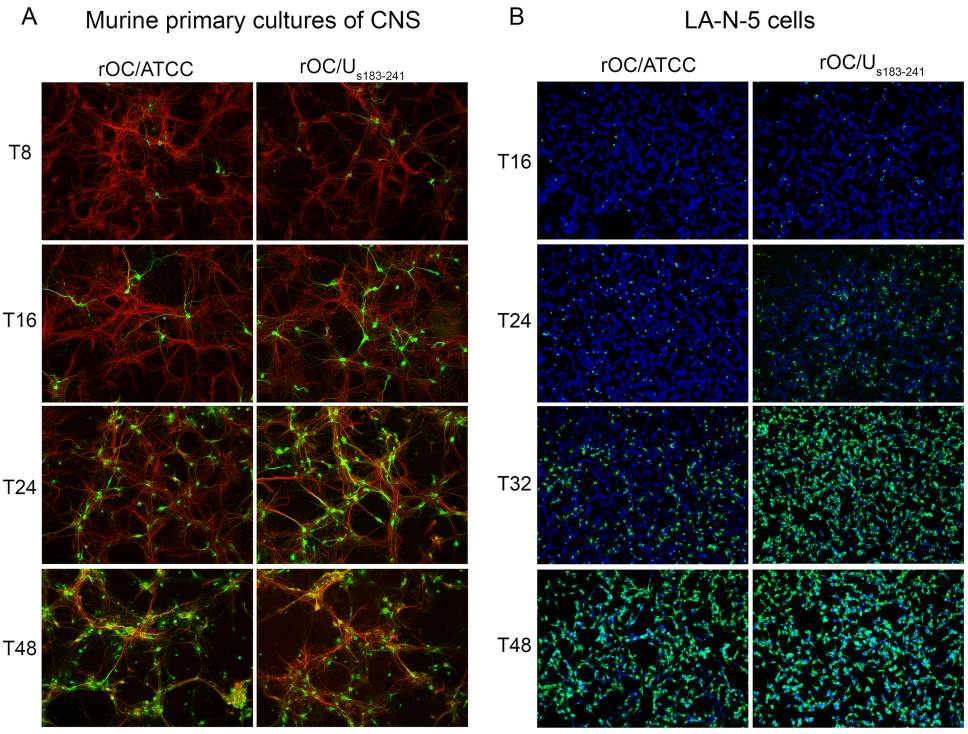


**FIG 3** rOC/$U_{s183/241}$ disseminates more rapidly than rOC/ATCC in neuronal cell cultures. Viral spreading was evaluated by immunofluorescence (IF). (A) Murine primary cultures of CNS infected at an MOI of 0.005 with both viruses at different times postinfection (T8 indicates 8 hpi, T16 is 16 hpi, etc.). Neurons (red) were stained with a MAb against microtubule-associated protein 2 (MAP2), and the S viral protein (green) was detected with a rabbit antiserum. (B) Differentiated human neuroblastoma LA-N-5 cells infected at an MOI of 0.2 with both viruses at different times postinfection. Cells were stained with a MAb against S viral protein (green), and DAPI (blue) was used to observe the nucleus. Results are representative of two independent experiments. Magnification, ×100.

hippocampus (Fig. 2B). Both viruses induced mild and similar activations of astrocytes at 5 dpi; however, unlike the reference virus, infection with the S mutant virus maintained a moderate activation of astrocytes until 7 dpi.

**rOC/$U_{s183–241}$ disseminates more rapidly than rOC/ATCC virus in neuronal cell cultures.** In order to study the link between neurovirulent properties and neuronal cell death induced by either rOC/$U_{s183–241}$ or rOC/ATCC, we compared two neuronal cell culture models. To establish whether the murine mixed primary CNS cultures and human LA-N-5 cells were susceptible at the same rate to the infection between rOC/ATCC and rOC/$U_{s183–241}$, the kinetics of viral spread were evaluated by immunofluorescence up to 48 hours postinfection (hpi) (Fig. 3). In murine primary cultures of CNS, the mutant virus spread more rapidly than the wild-type virus in neurons, as seen at 16 and 24 hpi (Fig. 3A). Although neurons are the primary target of infection in murine primary cultures, astrocytes were also infected later during infection by both viruses (data not shown). As observed in Fig. 3B, the mutant virus also spread more rapidly than the wt virus in LA-N-5 cells up to 32 hpi, a time when LA-N-5 cultures were almost all infected by rOC/$U_{s183–241}$ compared to only approximately 50% infection by the wt virus. The difference in viral spread is similar to those observed by histological examination in the CNS of infected BALB/c mice (Fig. 2A).

**rOC/$U_{s183–241}$ infection increases neuronal cell death in correlation with more infectious particle production.** Given that the S mutant virus was more neurovirulent and was able to spread faster than the wt virus in the mouse CNS and in neuronal cell cultures, we sought to evaluate whether the neuropathogenesis could be related to neuronal cell death. Even though both viruses induced cell death in murine mixed primary cultures of CNS and human LA-N-5 cells, the mutant virus was significantly more cytotoxic than the wt virus, as seen in Fig. 4A and B, respectively. The production

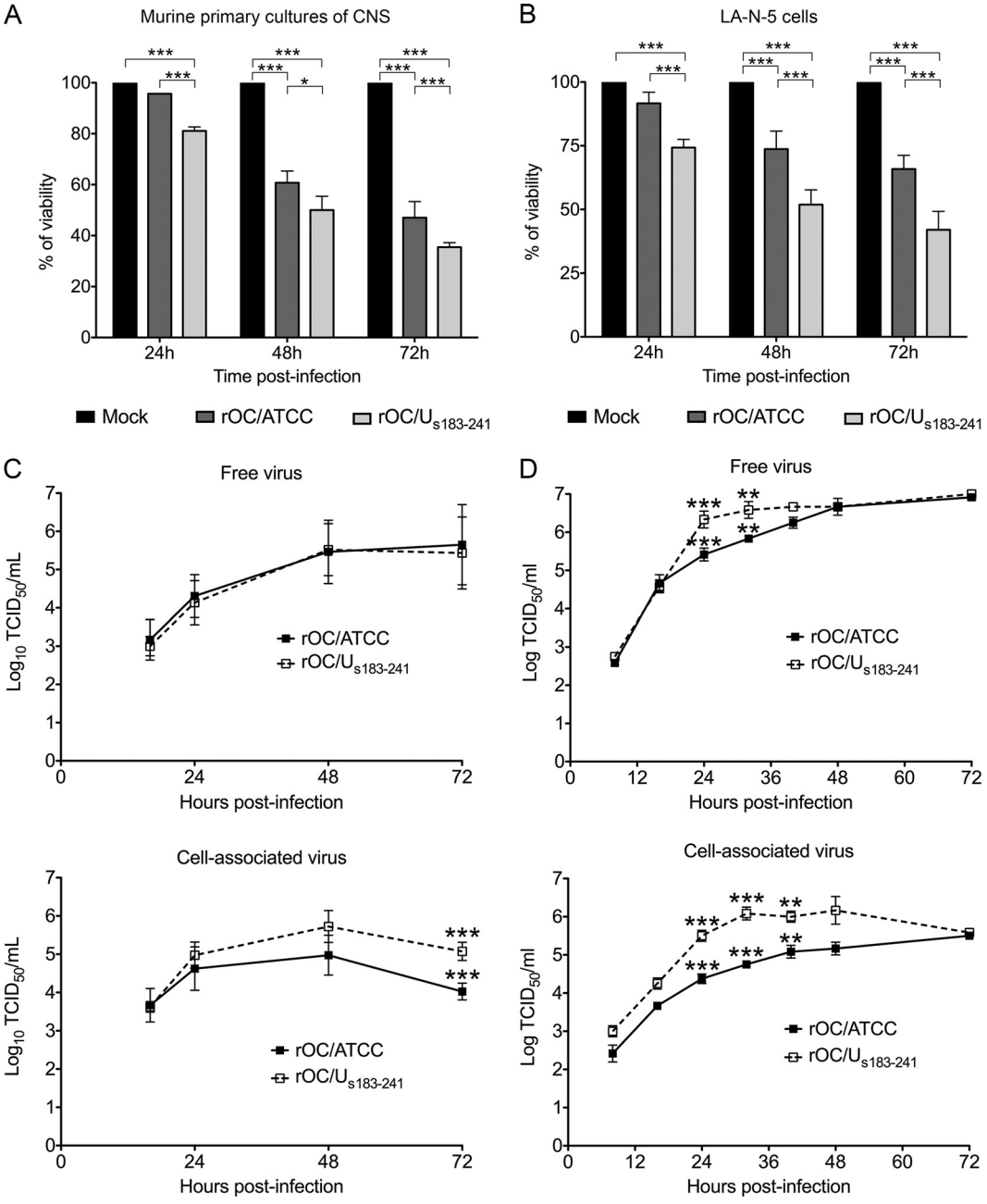


**FIG 4** rOC/$U_{s183–241}$ infection increases neuronal cell death and produces more infectious particles than rOC/ATCC infection. (A and C) Murine mixed primary cultures of CNS from BALB/c mice were infected with rOC/ATCC or rOC/$U_{s183–241}$ at an MOI of 0.03. (B and D) Differentiated human neuroblastoma LA-N-5 cells were infected with rOC/ATCC or rOC/$U_{s183–241}$ at an MOI of 0.2. (A) Cell viability was measured by MTT assay at the indicated time postinfection and expressed as relative percentages compared to mock-infected culture at each time point. (B) Cell viability was measured by PrestoBlue assay at the indicated times postinfection and expressed as relative percentages compared to mock-infected cells at each time point. (C) Production of infectious viral particles of free virus (upper) and cell-associated virus (lower) from mixed primary cultures of CNS (C) and LA-N-5 cells (D). Results are shown as means ± SD from three independent experiments. Statistical significance is indicated by asterisks: *, $P < 0.05$; **, $P < 0.01$; ***, $P < 0.001$.

level of infectious viral particles in cell culture medium (free virus) was significantly higher for mutant virus in LA-N-5 cells, whereas no difference was observed in primary cultures (Fig. 4C and D, upper); however, there was a significant increase of cell-associated infectious particle production for rOC/$U_{s183–241}$ compared to rOC/ATCC virus for both types of cell cultures (Fig. 4C and D, lower). Taken together, these results indicate that for both neuronal cell cultures, the infection with the mutant virus

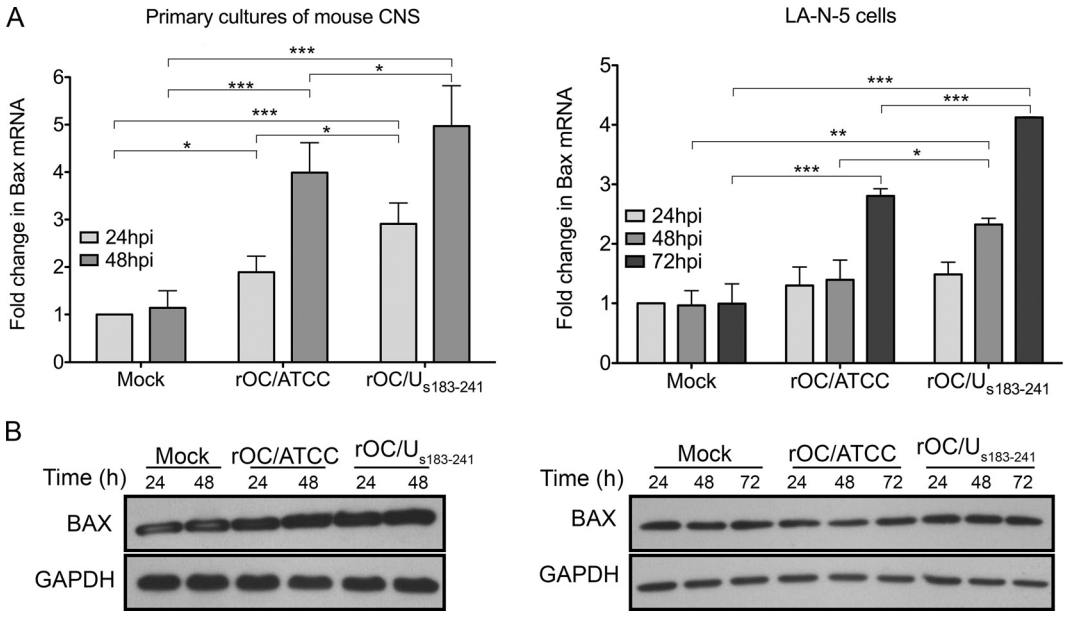


**FIG 5** Bax gene expression is increased in neuronal cell cultures during neuronal response to HCoV-OC43 infection. (A) Level of Bax mRNA in murine mixed primary cultures of CNS (left) or differentiated human neuroblastoma LA-N-5 cells (right) infected with rOC/ATCC or rOC/$U_{s183-241}$ was measured by quantitative real-time PCR (qPCR) at the indicated times postinfection. Results are shown as means ± SD from three independent experiments. Statistical significance is indicated by asterisks: *, $P < 0.05$; **, $P < 0.01$; ***, $P < 0.001$. (B) Results are representative of three independent experiments. Detection of Bax protein in murine mixed primary cultures of CNS (left) or differentiated human neuroblastoma LA-N-5 cells (right) infected with rOC/ATCC or rOC/$U_{s183-241}$ at the indicated times was performed by Western blot analysis (WB).

produced more infectious particles that led to an increase in neuronal cell death compared to the infection with the wild-type virus.

**Bax-dependent apoptosis does not play a significant role in neuronal cell death following HCoV-OC43 infection.** To further our understanding of the difference in cytotoxicity between viruses (Fig. 4 and reference 14) and to further characterize the neuronal response associated with RCD after infection, we sought to identify which cellular factors were involved in both neuronal cell models and to evaluate their relative importance after infection by either virus. Bax-dependent apoptosis is one of the best-described cell death pathways, and we have previously reported that Bax was relocalized to mitochondria after HCoV-OC43 infection (14). As the regulation of this proapoptotic factor can also be at the transcriptional level (35, 36), we evaluated its mRNA level and found that infection induced a significant increase in Bax gene expression between 48 hpi and 72 hpi for both viruses (Fig. 5A). Infection with the mutant virus led to a significantly higher increase in Bax gene expression compared to the wt virus, which correlated with the stronger induction of neuronal mortality in both neuronal cell cultures (Fig. 4A and B). On the other hand, the level of Bax protein remained stable and did not correlate with the increase in mRNA (Fig. 5B).

Since neuronal response to infection led to an increased expression of the Bax gene, and because we already showed that the corresponding protein was relocated to the mitochondria (14), we sought to evaluate the role of this factor in neuronal cell death. Interestingly, even the most efficient knockdown of Bax expression (Fig. 6A, population of short hairpin RNA [shRNA] Bax #1) did not protect LA-N-5 cells from damages induced by rOC/ATCC or rOC/$U_{s183-241}$ infection at 48 hpi compared to the control, as seen by the same cytopathic effect (rounding of cells and loss of axon are indicated by arrowheads and arrows, respectively) (Fig. 6B, left). In order to verify the functionality of the Bax protein, we assessed the morphology of LA-N-5 cells in the presence of staurosporine (STS) or infected by vesicular stomatis virus (VSV), both known to induce apoptosis through a Bax-dependent cell death pathway (37, 38). Knockdown of Bax expression with shRNA #1 abolished the cytopathic effect induced by STS or VSV, as

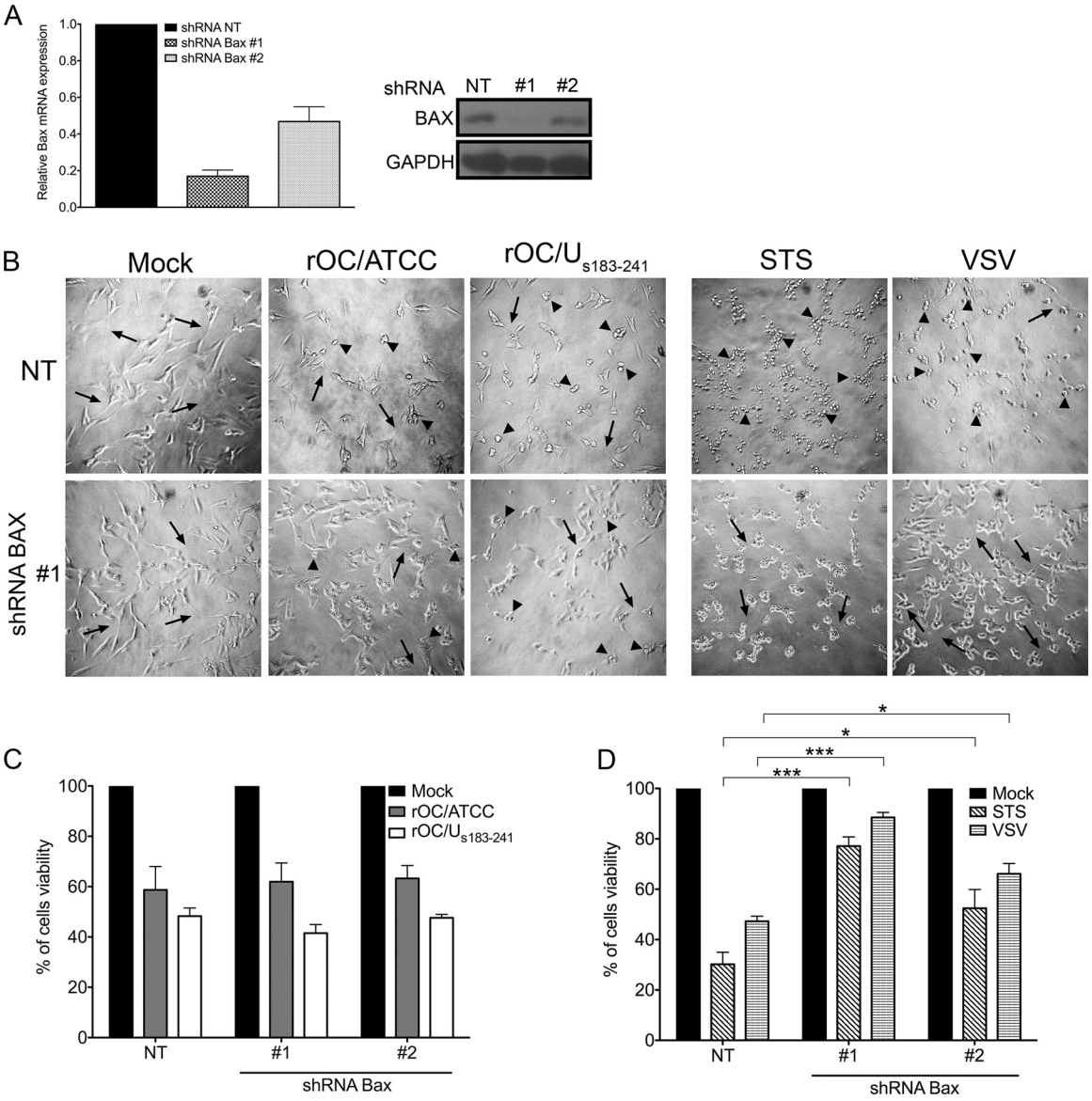


**FIG 6** Bax-dependent apoptosis does not play a significant role in LA-N-5 cell death induced by HCoV-OC43 infection. (A to D) Human neuroblastoma LA-N-5 cells were transduced with control lentivirus (NT) or lentivirus containing either of two shRNA sequences against Bax (shRNA Bax #1 or #2). (A) mRNA and protein expression of Bax was analyzed by qPCR (left) and WB (right). (B) Images of phase-contrast microscopy corresponding to differentiated LA-N-5 cells expressing shRNA NT or Bax #1 infected with rOC/ATCC or rOC/$U_{s183-241}$ at 48 hpi, treated with staurosporine (STS), or infected with vesicular stomatis virus (VSV) at 24 hpi. Arrows represent loss of axons or dendrites, and arrowheads indicate rounding of cells. (C) LA-N-5 cell viability was measured by PrestoBlue assay and expressed as relative percent viability compared to mock-infected cells at 48 hpi. (D) Cell viability was measured by PrestoBlue assay and expressed as relative percent viability compared to mock-infected cells. Differentiated LA-N-5 cells transduced with the different shRNAs were infected with VSV or treated with STS for 24 h. (A and B) Results are representative of two independent experiments. (C and D) Results are shown as means ± SD from two independent experiments. Statistical significance is indicated by asterisks: *, $P < 0.05$; **, $P < 0.01$; ***, $P < 0.001$.

seen at 24 hpi, and reduced the retractions of axons and dendrites (Fig. 6B, right), whereas the protection of neurons was moderate for population shRNA 2 (mild inhibition of Bax expression) following treatment with STS or VSV (data not shown). In order to quantify the apparent absence of cellular protection in populations infected with rOC/ATCC or rOC/$U_{s183-241}$, we measured cell viability and confirmed that Bax knockdown did not confer any protection against neuronal cell death induced during HCoV-OC43 infection (Fig. 6C), even though this knockdown led to strong protection against neuronal cell death induced by STS or VSV at 24 hpi in a dose-dependent manner compared to the control population (Fig. 6D). Together, these results indicate

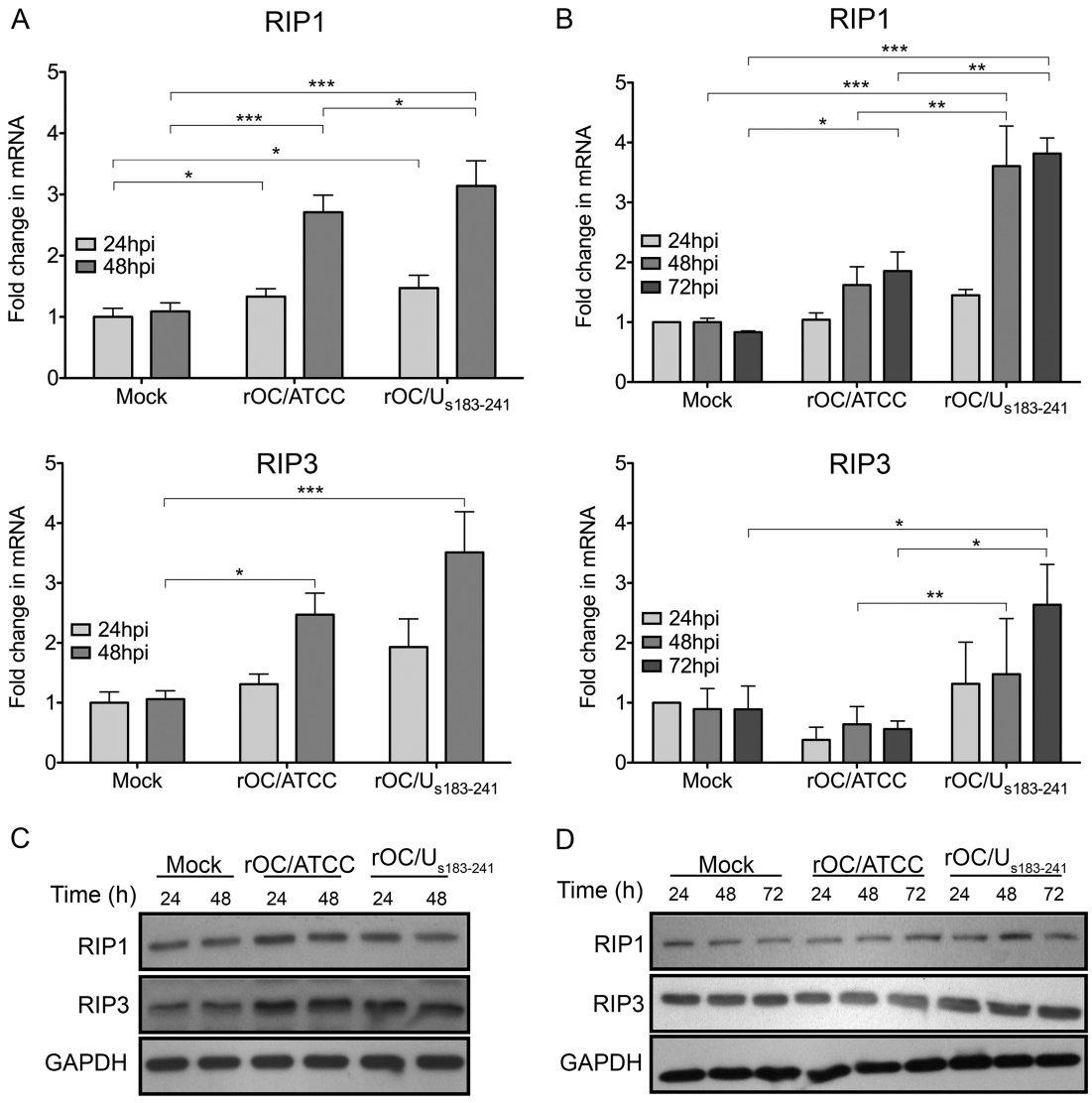


**FIG 7** HCoV-OC43 infection increases RIP1 and RIP3 gene expression. Level of RIP1 (upper) or RIP3 (lower) mRNA in murine mixed primary cultures of CNS (A) or differentiated LA-N-5 cells (B) infected with rOC/ATCC or rOC/$U_{s183-241}$. Results are shown as means ± SD from three independent experiments. Statistical significance is indicated by asterisks: *, $P < 0.05$; **, $P < 0.01$; ***, $P < 0.001$. (C and D) Detection of RIP1, RIP3, and GAPDH proteins in murine primary cultures of CNS (C) or differentiated LA-N-5 cells (D) infected with rOC/ATCC or rOC/$U_{s183-241}$ at the indicated times. Results are representative of three independent experiments.

that the proapoptotic factor Bax is functional in the LA-N-5 neuronal cells but does not play a significant role in HCoV-OC43-induced neuronal cell death.

**HCoV-OC43 infection induces an increase in RIP1 and RIP3 gene expression.** To further investigate RCD following coronavirus infection of neuronal cells and again evaluate whether there was a difference between viruses, we explored the possible involvement of receptor-interacting protein kinase 1 and 3 (RIP1 and RIP3) (29, 39), which are largely associated with necroptosis and potentially involved in neurological diseases or viral infections (40–43). In murine primary cultures of CNS, an increase in RIP1 (Fig. 7A, upper) or RIP3 (Fig. 7A, lower) mRNA was detectable at 48 hpi for both viruses compared to mock-infected cultures, even though rOC/$U_{s183-241}$ infection tended to transcribe more RIP1 and RIP3 mRNA. On the other hand, there was no significant increase in the level of corresponding proteins following infection with either virus, compared to mock infection, in murine primary cultures of CNS (Fig. 7C). In LA-N-5 cells, an increase in RIP1 and RIP3 mRNA was observed for mutant infection

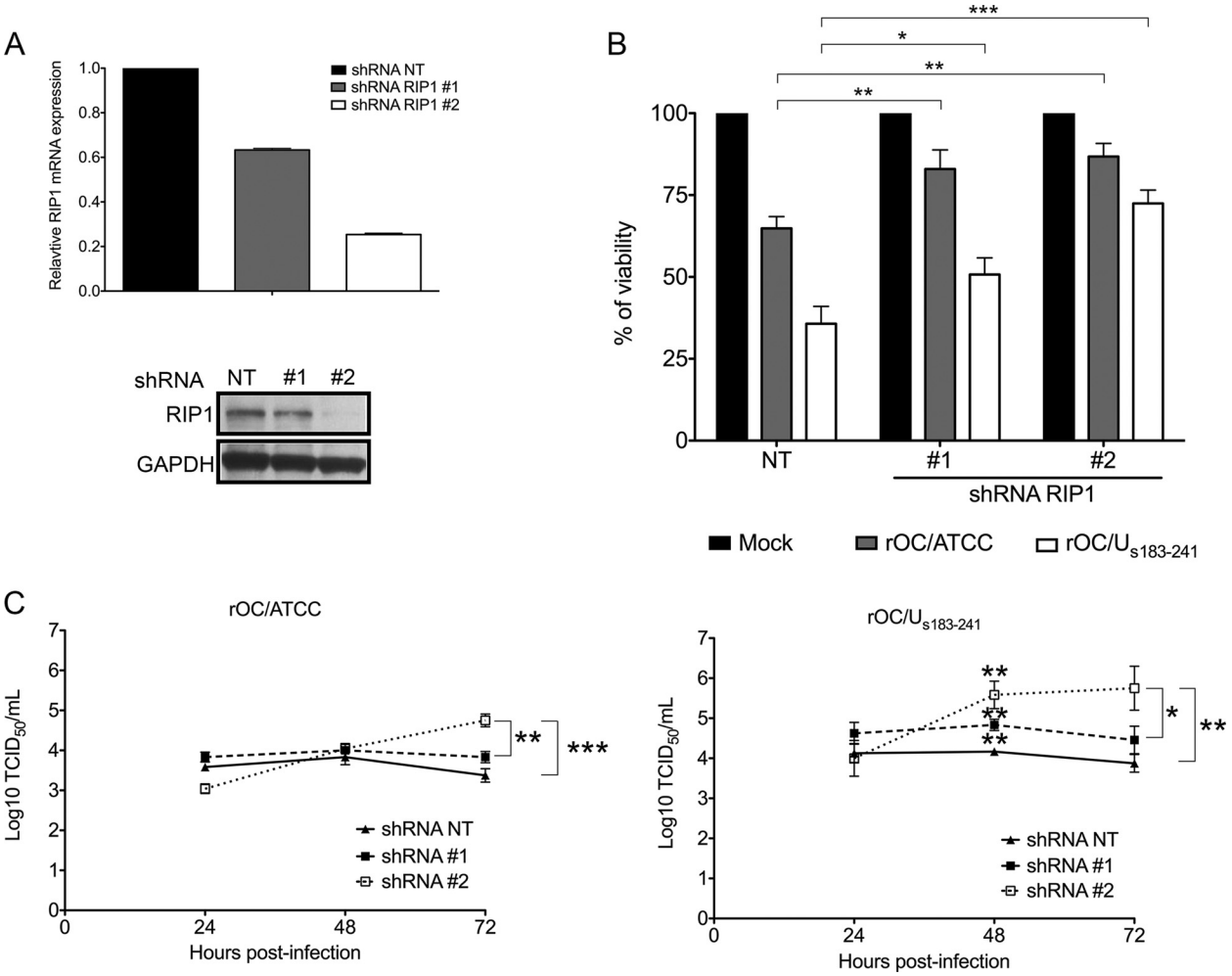


**FIG 8** RIP1 is involved in HCoV-OC43-induced LA-N-5 cell death and limits production of infectious virus. Differentiated LA-N-5 cells were transiently transduced with control lentivirus (shRNA NT) or lentivirus containing either of two shRNA sequences against RIP1 (shRNA RIP1 #1 or #2). (A) Expression of RIP1 was analyzed by qPCR (upper) and WB (lower). Results are representative of three independent experiments. (B) Cell viability was measured by PrestoBlue assay and expressed as relative percent viability compared to mock-infected cells at 72 hpi. (C) Production of cell-associated infectious viral particles for rOC/ATCC or rOC/$U_{s183-241}$ at the indicated times postinfection. Results are shown as means ± SD from three independent experiments. Statistical significance is indicated by asterisks: *, $P < 0.05$; **, $P < 0.01$; ***, $P < 0.001$.

compared to mock infection, whereas wild-type virus infection induced a modest increase in RIP1 gene expression only (Fig. 7B). Surprisingly, our results of Western immunoblotting showed that the amount of RIP1 protein did not increase following wt or mutant infection compared to mock infection of LA-N-5 cells (Fig. 7D), even if the corresponding gene expression was upregulated at 48 and 72 hpi (Fig. 6B). Similar to RIP1, RIP3 protein expression was stable during wt or mutant virus infection.

Inhibition of RIP1 and MLKL protects against neuronal cell death induced by both HCoV-OC43 variants and increases viral replication. Given that neuronal response to HCoV-OC43 infection induced an increase in RIP1 gene expression, an observation usually associated with necroptosis (44), we sought to evaluate the importance of this cell death pathway in neuronal cell death and viral production. By using RNA interference (RNAi) to knock down the expression of RIP1, we transduced LA-N-5 cells with two different shRNAs (#1 and #2) and quantified the amount of RIP1 mRNA and protein (Fig. 8). Quantitative PCR and Western blotting revealed that shRNA #2 was more efficient at knocking down expression of RIP1 (Fig. 8A). Inhibition of RIP1 by knockdown decreased the HCoV-OC43-induced cell death at 72 hpi in a dose-dependent manner compared to that of infected LA-N-5 cells transduced with control shRNA (NT) (Fig. 8B). As expected, inhibition of RIP1 expression protected LA-N-5 cells more efficiently against wt virus

infection than mutant infection, as the mortality rate induced by the latter is more important. In addition, to establish if viral replication was affected following cellular protection conferred by RIP1 knockdown, we quantified the production of wt and mutant infectious viral particles. Surprisingly, a significant increase in cell-associated mutant infectious particle production was observed at 48 and 72 hpi, when RIP1 expression was reduced (Fig. 8C). In fact, in the LA-N-5 cells transduced with the most efficient shRNA for knocking down RIP1 expression (shRNA #2), almost 50-fold more rOC/ATCC particles and 100-fold more rOC/$U_{s183–241}$ particles were harvested compared to levels from cells that had been transduced by nontarget shRNA. Thus, these results indicate that a reduction of RIP1 expression delayed neuronal cell death induced by both viruses, allowing an increase in the production of cell-associated infectious viral particles.

To further describe the cascade of events possibly associated with necroptosis and involving RIP1 during neuronal cell death induced by HCoV-OC43, we studied the activation of the factor MLKL, a known downstream effector that acts as an ion channel, which disturbs the osmotic homeostasis and disrupts the integrity of the plasma membrane (32, 45). Necrosulfonamide (NSA), a chemical inhibitor of MLKL, significantly increased the survival of LA-N-5 cells infected by either virus, suggesting a role for MLKL in neuronal cell death induced by HCoV-OC43 (Fig. 9A). Following infection of LA-N-5 cells by the mutant virus, NSA increased survival up to 86% compared to dimethyl sulfoxide (DMSO)-treated cells, for which viability was only 44.5%. Inhibition of MLKL also protected cells against mortality during infection with the reference virus by increasing viability by 30% compared to DMSO-treated cells. Inhibition of MLKL activation did not interfere with viral replication (Fig. 9B). To confirm the activation of MLKL following HCoV-OC43 infection, we proceeded by detecting its phosphorylated form. Indeed, phosphorylated MLKL was observed only after infection, whereas in the presence of NSA, both infections showed less phosphorylation of MLKL (Fig. 9C). Following activation, MLKL is known to homo-oligomerize and to translocate to the plasma membrane; therefore, we sought to evaluate if this was the case during HCoV-OC43 infection. We infected LA-N-5 cells with the reference or mutant virus, and then the cells were labeled with antibody against the N-terminal epitope of MLKL without previous membrane permeabilization to ensure that staining detected only the protein inserted into the plasma membrane with the N-terminal epitope of MLKL located on the outer side of the membrane. Confocal microscopy revealed that MLKL was at the cell surface after HCoV-OC43 infection, unlike the case for mock-infected cells (Fig. 9D), and that this translocation to the cell surface was more important after infection by the mutant virus. Together, these results indicate that MLKL is involved in neuronal cell death following HCoV-OC43 infection and that this activation is more substantial during infection by the S mutant virus than the wt virus.

## DISCUSSION

The human coronavirus OC43 (HCoV-OC43) has been demonstrated to be more than just a respiratory pathogen, as it possesses neuroinvasive and neurotropic properties, which raises interest in studying the potential relationship between HCoV-OC43 and neurological disease (10, 11). In the current study, we demonstrated that neurovirulent HCoV-OC43 infection leads to a neuronal response associated with the activation of regulated cell death (RCD). Moreover, two point mutations in the spike (S) glycoprotein (H183R and Y241H) are sufficient to accelerate viral dissemination as well as neuronal cell death. Accordingly, we introduced these mutations in the infectious cDNA clone of HCoV-OC43 (pBAC-OC43$^{FL}$) to produce a recombinant mutated rOC/$U_{s183–241}$ virus. Activation of the necroptosis-like pathway may represent a neuronal response to HCoV-OC43 infection to limit viral propagation but could also result in deleterious consequences associated with neuronal loss and neuropathology in the infected host.

Several neurotropic viruses, such as HIV, herpes simplex virus 1 (HSV-1), and influenza A virus (IAV), were reported to induce neuronal insults such as protein aggregates, oxidative stress, ER stress, and synaptic alterations during infection, all

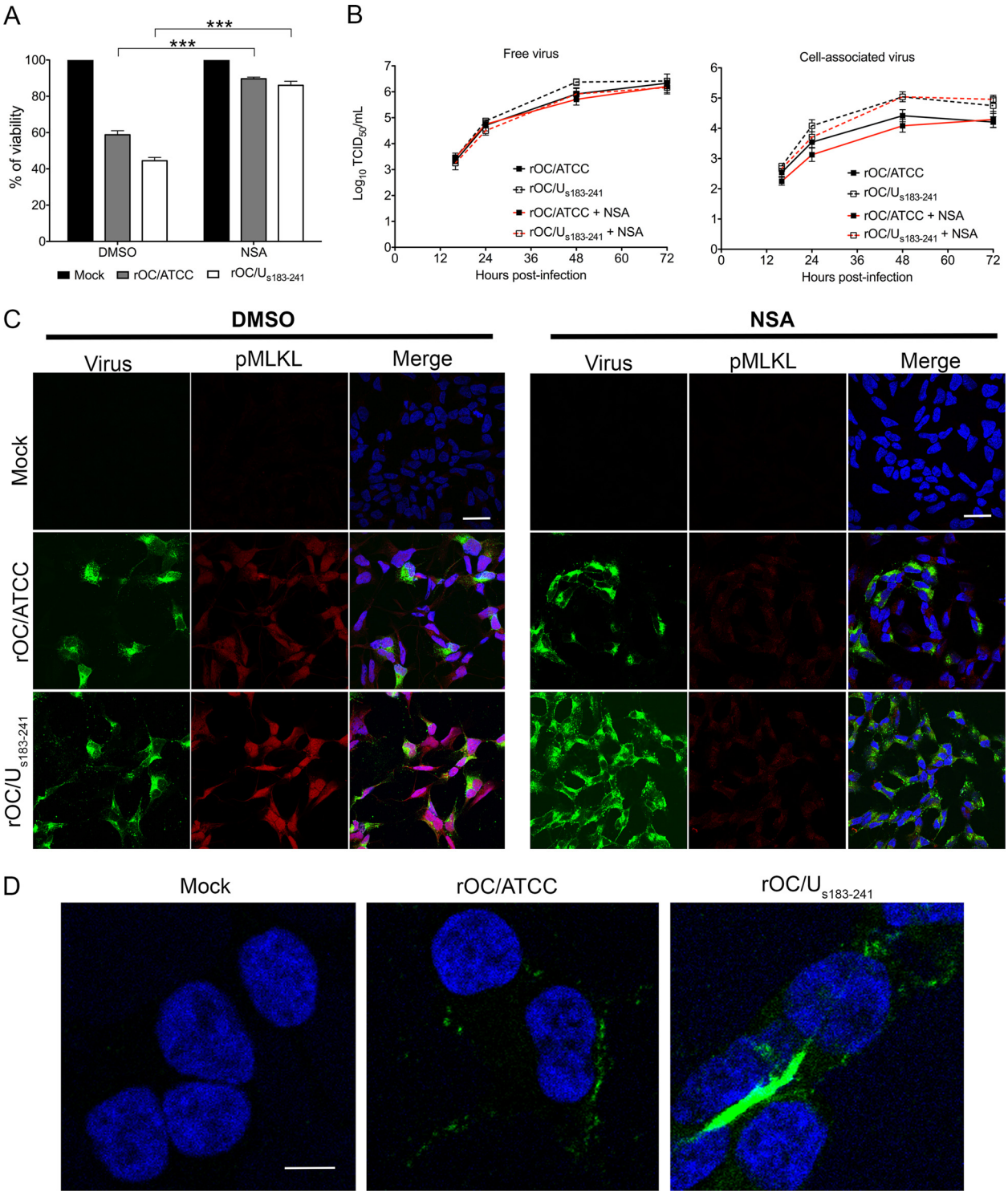


**FIG 9** MLKL is involved in LA-N-5 cell death induced by HCoV-OC43. (A) Differentiated LA-N-5 cells were infected with rOC/ATCC or rOC/$U_{s183-241}$ at an MOI of 0.2 and then treated with 2 $\mu$M NSA or DMSO. Cell viability was measured by PrestoBlue assay and expressed as relative percent viability compared to mock-infected cells at 72 hpi. (B) Production of infectious free virus (left) or cell-associated virus (right) for rOC/ATCC or rOC/$U_{s183-241}$ at the indicated times postinfection. (C) Differentiated LA-N-5 cells were treated with 2 $\mu$M NSA or left untreated (DMSO) after infection with rOC/ATCC or rOC/$U_{s183-241}$ at an MOI of 1. Phosphorylated MLKL was stained in red, viral S glycoprotein in green, and nucleus in blue and observed by confocal microscopy. Scale bar, 5 $\mu$m. (D) Differentiated LA-N-5 cells were infected with rOC/ATCC or rOC/$U_{s183-241}$ at an MOI of 1. The surface distribution of MLKL (green) and nucleus (blue) were detected by confocal microscopy. Scale bar, 20 $\mu$M. For panels A and B, data are represented as means $\pm$ SD and were obtained from three independent experiments. Statistical significance is indicated by asterisks: ***, $P < 0.001$. For panels C and D, images shown are representative of two independent experiments.

contributing to neuropathogenesis (46–48). Indeed, neurons in the CNS are particularly vulnerable to intracellular dysfunction where protein misfolding or synaptic alterations could result in neuronal loss (49–52). Our previous studies demonstrated that rOC/$U_{s183–241}$ infection enhanced the unfolded protein response (UPR) and protein synthesis inhibition (13), suggesting that this mutant virus could increase ER stress in neurons associated with neurodegeneration and neuropathogenesis in infected mice. These observations can also relate to other data which demonstrated that HCoV-OC43 interferes with neurotransmitter homeostasis and induces glutamate excitotoxicity (15, 16), thus promoting neuronal stress and eventual neuropathogenesis in infected mice.

Here, our results indicate that the S mutant rOC/$U_{s183–241}$ acquired the capacity to disseminate more rapidly and to produce more infectious particles than the reference virus in the CNS of infected mice as well as in neuronal cell cultures, resulting in an increased neurovirulence and induction of cell death (Fig. 1 to 4). Moreover, mutations in the viral S protein appear to modulate the neuronal cellular response involving inflammation, neuronal damage, and eventually loss of neurons by RCD activation, as seen in other viral infections, such as MHV, HSV-1, and flavivirus (53–55). Indeed, RCD is sometimes known to favor a proinflammatory environment and contribute to neuroinflammation by mediating the release of damage-associated molecular patterns (DAMPs) and production of proinflammatory cytokines (56, 57). We previously reported that HCoV-OC43 infection leads to the production of proinflammatory cytokines, such as interleukin-1 (IL-1), TNF-$\alpha$, and IL-6, and T-lymphocyte infiltration ($CD4^+$ and $CD8^+$) in the CNS (17). This, together with the increased astrogliosis observed in the CNS of S mutant-infected mice (Fig. 2B), suggests that infection by this mutant virus contributes to enhanced proinflammatory cytokine secretion and to a deleterious neuroinflammation process. Similarly, neurovirulence of the murine coronavirus MHV-A59 was linked to the excessive production of proinflammatory cytokines by astrocytes and microglial cells in brain and spinal cord of infected mice (58).

Apart from activation of neuroinflammation and neuronal damage, RCD activation during HCoV-OC43 infection also could serve to restrict pathogen spread. We previously demonstrated that HCoV-OC43 infection induced neuronal cell death in the mouse CNS (11). Despite the lack of precise identification of RCD, these results suggest that, while contributing to the elimination of infected neurons, RCD could participate in virus-initiated neuropathogenesis. Our data on neuronal cell death indicate that the infection by the mutant virus induces more neuronal cell death (Fig. 4). Surprisingly, even though we previously showed relocalization of the Bax protein to the mitochondria (14) and considering that the murine counterpart of HCoV-OC43, MHV, was reported to induce Bax-dependent apoptosis in oligodendrocytes (59, 60), the proapoptotic cellular factor Bax was not involved in neuronal cell death induced by HCoV-OC43. This suggests that during a coronavirus infection, this proapoptotic factor could be activated in a cell type-specific manner or that the human virus possesses specific strategies to subvert Bax-dependent apoptosis and evade this type of RCD activation. Although Bax-dependent apoptosis is often activated during infection in order to limit viral propagation (61–63), several viruses have acquired diverse strategies to block this form of RCD (64). Indeed, cytomegalovirus (65), myxoma virus (66), vaccinia virus (67), and Epstein-Barr virus (68) all encode viral Bcl-2 homologs that interact with and inhibit Bax activation. Until now, no HCoV-OC43 proteins have been shown to have antiapoptotic properties, and further studies are warranted to explore how HCoV-OC43 could interfere with Bax-dependent apoptosis in neuronal cells. On the other hand, it was already reported that some intracellular oxidative alterations could result in translocation of Bax to the mitochondria without any signs of apoptosis activation (69). As several viruses are known to destabilize the cellular redox state during infection (70–72), it is possible that HCoV-OC43 infection induces a redox imbalance, promoting translocation of Bax to the mitochondria without any consequences on neuronal cell death.

Other types of RCD are now well described and are activated by different stimuli (21). Necroptosis is now considered an alternative RCD pathway mostly involved when

caspase-8-dependent apoptosis is inhibited or altered or when endogenous RIP3 expression is high enough to sensitize cells to necroptosis activation (73). Moreover, many neurological disorders, such as amyotrophic lateral sclerosis (74), Huntington's disease (75), multiple sclerosis (76), and ischemic brain injury (77), may be related to necroptosis activation, as observed by significant expression or activity of RIP1, RIP3, and MLKL (78). The expression and activation of these factors are also considered to be a defense mechanism against pathogen invasion (64, 79). Several viruses, such as HIV (80), reovirus (81), IAV (82), CMV, and HSV (83), are known to activate RIP1, RIP3, or MLKL in cells. On the other hand, HSV-1, HSV-2, and CMV are also able to interfere with necroptosis to block cell death (84, 85). Our results show that infection of neuronal cultures by the S mutant virus leads to an increase in RIP1 and RIP3 transcription compared to that of wt virus. As the S mutant virus disseminates faster, this could be due to an increased number of infected neurons that are engaging a pronecroptotic response as well as the fact that these mutant-infected cells produce more infectious particles (Fig. 4 and reference 13), which could induce a more intense disruption of cell homeostasis and, in the end, trigger a stronger activation of RIP1 and RIP3. Furthermore, as previously suggested (14), the faster spreading and increased production of viral particles by the S mutant virus may also implicate other viral factors involved in the regulation of RCD that are produced in larger amounts than wild-type virus as well as other host cell factors. Even though there were no corresponding increased amounts of RIP proteins, our results clearly indicate that RIP1-associated RCD plays a role in HCoV-induced cell death, as seen by significantly increased survival of infected LA-N-5 cells in which RIP1 has been knocked down (Fig. 8B). Moreover, inhibition of RIP1 expression also results in an increase of cell-associated infectious particle production (Fig. 8C), suggesting that RIP1 is activated by neurons in response to the infection as an attempt to restrict viral replication. MLKL represents the major executioner factor in the necroptotic pathway; therefore, the significantly increased survival of LA-N-5 cells in the presence of an MLKL inhibitor (NSA) and MLKL phosphorylation and relocalization at the surface of the neurons (Fig. 9) suggest that necroptosis-like pathways related to RIP1 and MLKL were involved in the cell death induced by HCoV-OC43. Recently, Nogusa and colleagues showed that RIP3 can activate both MLKL-driven necroptosis and FADD-mediated apoptosis in IAV-infected cells to restrict viral propagation and suggested that this process does so by reducing viral replication in infected cells and promoting activation of immune cells associated with the release of DAMPs from dying cells (82). This is in accordance with our hypothesis that the necroptotic process engaged during HCoV-OC43 infection serves to activate immunity. On the other hand, this caspase-dependent proapoptotic role of RIP3 during IAV infection is highly interesting, as necroptosis and apoptosis are often seen as mutually exclusive alternative forms of RCD. Considering this observation, even though Bax-mediated apoptosis (Fig. 6) and caspases (14) are clearly not involved during neuronal cell death in our model, we cannot rule out that, in parallel to necroptosis, other forms of RCD also participate during neuronal cell infection by HCoV-OC43.

As described before (13), HCoV-OC43 induces an ER stress associated with the activation of some components of the UPR system, including GRP78. The induction of ER stress and activation of GRP78 were previously reported to precede and lead to necroptosis activation by an unknown mechanism (86, 87). Therefore, one can hypothesize that infection by HCoV-OC43 induced an ER stress in neurons that initiate RIP1-MLKL-driven necroptosis. Furthermore, inhibition of cyclophilin D, an isomerase acting to modulate the mitochondrial permeability transition pore, has been shown to reduce necroptosis-related cell death in mouse embryonic fibroblasts (88, 89). We previously reported that inhibiting cyclophilin D in HCoV-OC43-infected LA-N-5 cells partially protects neurons from cell death, supporting the hypothesis that this factor is also at least partially involved in the RIP1-MLKL necroptosis-like pathway. In sum, HCoV-OC43-induced RCD appears to involve several host cell factors and potential cross talk between signaling pathways that implicate necroptosis. Further studies are ongoing to continue to characterize the cascade of events that takes place during the

process and whether the mutations in the viral S protein engage other pathways in infected cells.

The current study demonstrates that two point mutations located in the viral S glycoprotein are sufficient to increase the neurovirulence of HCoV-OC43 in mice. Again, by improving the capacity of the mutant virus to produce more infectious particles and disseminate more efficiently, these mutations seem to engage an increased activation of the RIP1-MLKL necroptosis-like pathway. Therefore, it is reasonable to think that host cells respond to HCoV-OC43 infection within the CNS by engaging a necroptosis-like pathway in order to clear or at least limit the infection in cases where other types of RCD (like Bax-dependent apoptosis) are unable to accomplish this function. However, when infection triggers a stronger activation of this necroptosis-like pathway (mutant versus wild-type virus), it may induce an excessive neuroinflammation associated with an enhanced release of DAMPs (37, 79), and the cellular response to the infection may become deleterious for the host. Depending on the viral infection within the CNS, the neuronal responses may engage specific factors or pathways of RCD to clear the pathogens but at the same time generate damage that increases susceptibility to neurological disorders for the host. The challenge will be to target and modulate specific RCD activation without interfering in antiviral responses within the CNS to attenuate the deleterious effect following neuronal cell death and improve long-term strategies for CNS protection against neurological diseases.

## MATERIALS AND METHODS

**Ethics and biosafety statement.** All animal experiments were approved by the Institutional Animal Care and Use Ethics Committee (IACUC) of the Institut National de la Recherche Scientifique (INRS) and conform to the Canadian Council on Animal Care (CCAC). Animal care and use protocol numbers 1304-02 and 1205-03 were issued by the IACUC of INRS for the animal experiments described here. All of the experiments with both wild-type and mutant viruses (S protein with a potential gain of function) were approved by the institutional biosafety committee (IBC) at INRS (certificate 2013-07), as biosafety level 2 (BSL2) measures were applied to prevent infection of laboratory workers and potential spread of viruses.

**Cell lines, viruses, and reagents.** The human neuroblastoma LA-N-5 cell line (a kind gift from Stephan Ladisch, George Washington University School of Medicine, Washington, DC) was routinely cultured at 37°C with 5% $CO_2$ in RPMI (Life Technologies) supplemented with 15% (vol/vol) fetal bovine serum (FBS; GE Healthcare), 10 mM HEPES, 1 mM sodium pyruvate (NaPy), and 100 $\mu$M nonessential amino acids (Life Technologies). The LA-N-5 cells were differentiated into neurons as previously described (13, 90) for all experiments. Briefly, cells were seeded in RPMI supplemented with 15% (vol/vol) FBS, 10 mM HEPES, 1 mM NaPy, 100 $\mu$M nonessential amino acids, and the next day and every 2 days for a period of 6 days, 10 $\mu$M all-*trans*-retinoic acid (Sigma-Aldrich) was added to the same medium supplemented with 10% (vol/vol) FBS. The HRT-18 cells (kind gift from the late David Brian, University of Tennessee) were cultivated in minimal essential medium alpha (MEM-alpha; Life Technologies) supplemented with 10% (vol/vol) FBS.

The recombinant wild-type (wt) reference HCoV-OC43 (rOC/ATCC) virus and the recombinant mutant HCoV-OC43 virus (rOC/$Us_{183–241}$), containing two point mutations within the S spike glycoprotein (H183R and Y241H), were generated using a full-length cDNA clone as previously described (13, 91). LA-N-5 cells were infected at a multiplicity of infection (MOI) of 0.2 during 2 h at 37°C for adsorption and then incubated with RPMI supplemented with 2.5% (vol/vol) FBS for the indicated times postinfection. For infection of LA-N-5 cells with the wild-type Indiana strain of vesicular stomatis virus (VSV), an MOI of 1 was used and viruses were incubated in a minimal volume for 1 h at 37°C. The medium was replaced by RPMI with 2.5% (vol/vol) FBS, and then cells were incubated at the indicated times.

Staurosporine (STS) was purchased from Sigma-Aldrich and used to treat LA-N-5 cells at a final concentration of 500 nM, which were incubated overnight at 37°C. Necrosulfonamide (NSA) was purchased from Abcam and used at 2 $\mu$M.

**Mice, survival curve, body weight variation, and evaluation of clinical scores.** Twenty-two-day-old female BALB/c mice (Charles River Laboratories) were inoculated by the intracerebral route with $10^{2.5}$ 50% tissue culture infective doses ($TCID_{50}$) of wt or mutant virus, as previously described (17). Groups of 10 mice were subjected to observation on a daily basis for survival and body weight variations over a period of 22 days postinfection. Clinical scores were evaluated using a scale with 4 distinctive levels, as previously described (34). Briefly, asymptomatic mice were classified as level 0, level 1 was for mice with symptoms of abnormal flexion of the four limbs, level 2 was for mice presenting social isolation, ruffled fur, and hunched backs, and level 3 was attributed to mice that were in a moribund state or dead.

**Primary cultures of mouse CNS.** Embryos at 14 to 16 days of gestation were removed from pregnant anesthetized CD1 mice. The cortex and hippocampus of the embryonic pup brains were harvested and placed in Hanks balanced salt solution (HBSS) medium, without $Ca^{2+}$ and $Mg^{2+}$ but supplemented with 1.0 mM sodium pyruvate and 10 mM HEPES buffer. The tissues were incubated in 5 ml of a solution of HBSS and trypsin– 0.5% EDTA (ratio of 10:1, respectively) for 15 min at 37°C with gentle tilting to mix. After digestion, the tissues were washed for 5 min three times with HBSS, and the medium

was removed and replaced by fresh HBSS medium (without $Ca^{2+}$ and $Mg^{2+}$ but supplemented with 1.0 mM sodium pyruvate and 10 mM HEPES buffer). Tissues were gently pipetted up and down with a Pasteur pipette to dissociate the cells. After a decantation step of 5 min at room temperature, supernatants were then transferred into a 50-ml tube with 36 ml of Neurobasal medium (Life Technologies) supplemented with 0.5 mM GlutaMAX-I (Life Technologies), 10 mM HEPES buffer, B27 supplement (Life Technologies), gentamicin, and 10% horse serum. This step was performed twice to increase the final amount of cells. Cells were then seeded at approximately $1 \times 10^5$ cells/cm$^2$ and grown on collagen–poly-D-lysine (3:1, for a final concentration of 50 $\mu$g/ml)-treated glass coverslips for immunofluorescence assay in the same medium, which was replaced by fresh Neurobasal medium without horse medium the next day. The medium was changed every 2 days thereafter, and the cultures were ready for infection after 7 days in culture. For experiments where RNA/proteins or virus was harvested, cells were seeded without glass coverslips in 24- or 6-well plates, respectively.

**Cell viability assay.** The viability of LA-N-5 cells was monitored using PrestoBlue (Life Technologies) through reduction of resazurin-like reagent according to the manufacturer's protocol. Briefly, cells were plated at $2.5 \times 10^3$ per well, grown, and differentiated with all-*trans*-retinoic acid (Sigma-Aldrich) in Cell+ 96-well plates (Starstetd). After the indicated times postinfection, PrestoBlue was added in each well and optical density (OD) read as the difference between values at 570 nm and 600 nm every hour for 3 h with a microplate reader (Bio-Rad). Cell viability was determined according to slope regression analysis for each sample and compared to the slope from mock-infected cells. Cell viability of murine primary cultures of CNS was monitored using the reduction of 3-(4,5-dimethylthiazol-2-yl)-2,5-diphenyltetrazolium bromide dye (MTT assay) by following the manufacturer's instructions (Roche). Briefly, after the indicated times postinfection, 50 $\mu$l of MTT labeling reagent was added to primary cultures of mouse CNS seeded in 24-well plates containing 500 $\mu$l of Neurobasal medium. After incubation of cells at 37°C for 1 h, 550 $\mu$l of MTT solubilization buffer was added in each well, and then the wells were incubated at 37°C for 18 h. From each well of the 24-well plate, 200 $\mu$l was transferred to 5 new wells of 96-well plates and the OD was measured in replicates at 570 nm using a microplate reader (Bio-Rad).

**Quantification of infectious virus production by IPA.** Indirect immunoperoxidase assay (IPA) was performed to evaluate viral production as free virus (in the cell culture medium) and as cell-associated virus, as previously described (92). Briefly, serial dilution of infected LA-N-5 cell supernatant (free virus) or frozen/thawed whole-cell lysates (cell-associated virus) were added to HRT-18 cells seeded in 96-well plates and incubated at 37°C with 5% $CO_2$ for 4 days. The cells were washed once with phosphate-buffered saline (PBS) and fixed with methanol containing 0.1% (vol/vol) hydrogen peroxide. The primary antibody was the mouse monoclonal antibody (MAb) 4.3E4 (1/2), which was added to each well to detect viral S glycoprotein, and wells were incubated at 37°C with 5% $CO_2$ for 2 h and then washed three times with PBS. The cells were then incubated with the goat anti-mouse secondary antibody (KPL) conjugated with horseradish peroxidase at 37°C without $CO_2$ for 2 h and washed again with PBS three times. Immune complexes were detected with 0.2 mg/ml of 3,3′-diaminobenzidine tetrahydrochloride (DAB) (Sigma-Aldrich) and 0.01% hydrogen peroxide ($H_2O_2$) in PBS. Viral titers were analyzed by the Karber method, as previously described (92).

**RNA extraction, cDNA synthesis, and quantitative PCR.** Total RNA from cells was extracted using the RNeasy minikit (Qiagen) according to the manufacturer's protocol. Total RNA quantification was determined using a NanoDrop N-1000 spectrophotometer (Thermo Scientific), and cDNA synthesis was performed using a Superscript III first-strand kit (Life Technologies) with 2 $\mu$g of RNA according to the manufacturer's instructions. Detection and quantification of gene expression of each gene of interest were performed using specific primers and the SsoFast EvaGreen supermix (Bio-Rad). PCR products were detected and quantified using a Rotor-Gene 6000 quantitative real-time PCR (qPCR) instrument (Corbett Life Science).

**Protein extraction and Western immunoblotting.** Total proteins were extracted from whole-cell lysates in petri dishes (cells kept on ice) with a cell scraper (Sarstedt) and washed with 5 ml of PBS. Cells were centrifuged at 3,500 rpm for 5 min at 4°C and washed once with 1 ml of PBS. The cells were transferred to a microtube and centrifuged again at 3,500 rpm for 5 min at 4°C, and the pellet was resuspended in radioimmunoprecipitation assay (RIPA) buffer (0.15 mM NaCl, 1% [vol/vol] Nonidet P-40, 0.5% [wt/vol] deoxycholate, 0.1% [wt/vol] SDS, and 0.05 M Tris, pH 8.0) containing fresh protease inhibitor cocktail set I (Calbiochem). Cell lysates were incubated on ice for 20 min and centrifuged at 14,000 rpm for 10 min at 4°C. The supernatants were transferred to a new tube and conserved at −80°C for further analysis.

Protein concentrations were measured using the bicinchoninic acid (BCA) protein assay kit (Novagen) according to the manufacturer's protocol. Equal amounts of proteins were subjected to SDS-PAGE using 10% or 4 to 15% Criterion XT precast gels (Bio-Rad) and then transferred to a polyvinyl difluoride (PVDF) membrane (Bio-Rad) with a Trans-Blot semidry transfer cell apparatus. The membranes were blocked for 1 h at room temperature (RT) with 5%, wt/vol, nonfat milk in Tris-buffered saline containing 0.1% (vol/vol) Tween 20 (TBS-T) and incubated with TBS-T containing primary antibodies with 5% (wt/vol) skim milk at 4°C overnight. Western blot analyses were performed for detection of Bax, RIP1, RIP3, and glyceraldehyde-3-phosphate dehydrogenase (GAPDH) proteins using rabbit anti-human Bax antibody (1/2,000; sc-493; Santa Cruz Biotechnology), mouse anti-human/mouse RIP1 antibody (1/2,000; clone38; BD Biosciences), rabbit anti-human RIP3 antibody (1/2000; 27-361; ProSci), and rabbit anti-human GAPDH antibody (1/10,000; sc-25778; Santa Cruz Biotech), respectively, as primary antibodies. The membranes were washed three times with TBS-T at RT for 5 min before being incubated with anti-mouse or anti-rabbit secondary antibodies (GE Healthcare) coupled to horseradish peroxidase (HRP) for 1 h at RT. After three washes, the bands were visualized by chemiluminescence using Clarity Western ECL substrate (Bio-Rad), and loading was normalized to the housekeeping protein GAPDH.

**Lentivirus production, transduction, overexpressing clones, and generation of knocked down LA-N-5 cell populations.** Lentiviral pseudoparticles used for gene silencing were produced following transfection of HEK293T cells with pLP1, pLP2, pVSV-G (Sigma-Aldrich), and short hairpin RNA (shRNA) vectors. The Mission pLKO.1 shRNA vector against Bax (shRNA #1, TRCN0000312626; shRNA #2, TRCN0000312627), RIP1 (shRNA #1, TRCN00000705; shRNA #2, TRCN00000709), and the control shRNA (nontarget shRNA) were purchased from Sigma-Aldrich. Overall, $5 \times 10^6$ cells were plated in petri dishes precoated with sterile PBS containing 0.1% (vol/vol) gelatin. Cells then were cotransfected with 6 $\mu$g of each vector per petri dish and Lipofectamine 3000 (Life Technologies) according to the manufacturer's protocol. After 5 h, the medium was replaced by DMEM supplemented with 10% (vol/vol) FBS and then incubated for 96 h at 37°C with 5% $CO_2$. The supernatant was harvested and lentiviral pseudoparticles were concentrated using the Lenti-X Maxi purification kit (Clontech) before being purified and eluted in sterile PBS with PD-10 columns according to the manufacturer's protocol (GE Healthcare).

For the transient knockdown of RIP1 expression, LA-N-5 cells were differentiated into neurons with retinoic acid for 6 days, and lentiviral pseudoparticles were added to an MOI of 10. After 24 h, the medium was replaced with RPMI containing retinoic acid to complete the differentiation, and the cells were incubated for another 48 h before proceeding to infection with HCoV-OC43.

For stable Bax knockdown, undifferentiated LA-N-5 cells were transduced with Bax lentiviral pseudoparticles and cell populations were selected with 2 $\mu$g/ml puromycin after 24 h in RPMI supplemented with 20% (vol/vol) FBS. A population of LA-N-5 cells transduced with empty vector (EV) selected as previously described were used as reference cells. All populations of Bax knockdown LA-N-5 cells were maintained in RPMI plus 15% FBS supplemented with 1 $\mu$g/ml puromycin during all experiments. The expression level of Bax in all populations was analyzed by qPCR and Western blotting.

**Immunofluorescence/immunohistochemistry (IHC).** For immunofluorescence assay, cells were washed with sterile PBS and then fixed with 4%, wt/vol, paraformaldehyde (PFA; Fisher) for 30 min at RT. After another washing with PBS, cells were permeabilized with 100% methanol at −20°C for 5 min and washed once again with PBS. Cells were incubated with different primary antibodies, including mouse anti-spike HCoV-OC43 protein (1-10.C3) monoclonal antibody (1/2; hybridoma supernatant), polyclonal rabbit anti-S protein of bovine coronavirus (BCoV; 1/1,000), monoclonal mouse anti-microtubule-associated protein 2 (MAP2) antibody (1/1,000; 556320; BD Biosciences), polyclonal rabbit anti-glial fibrillary acidic protein (GFAP) antibody (1/1,000; Z0334; Dako), rabbit anti-MLKL (1/200; M6687; Sigma-Aldrich), and rabbit anti-phosphorylated MLKL (1/200; EPR9514; Abcam), for 1 h at RT and then washed three times with PBS. Cells were incubated for 1 h at RT with the secondary antibodies (Life Technologies) anti-mouse Alexa Fluor 488 (1/1,000), anti-rabbit Alexa Fluor 488 (1/1,000), anti-mouse Alexa Fluor 647 (1/1,000), and anti-mouse Alexa Fluor 568 (1/1,000) and then washed three times with PBS. Nuclei were detected with 4′,6-diamidino-2-phenylindole (DAPI) for 5 min at RT and washed once with PBS. For experiments with nonpermeabilized LA-N-5 cells, antibodies were diluted in cold medium (RPMI plus 5% FBS) and added to chilled cells on ice for 1 h before being washed twice with cold medium. Ice-cold cells then were incubated with secondary antibody diluted in cold medium for 1 h, washed, and fixed in 4% PFA for 20 min at RT.

For IHC, mice infected (wt or mutant virus) or left uninfected (sham) were perfused with 4%, wt/vol, PFA, and whole brains were carefully harvested from mice infected at 5, 7, and 9 days after intracerebral injection of each virus. Brain tissues were sectioned using a vibratome (VT1000E; Leica) to yield 60-$\mu$m sections. Prior to staining, sections were incubated with a solution of two droplets of $H_2O_2$ in PBS for 10 min at RT and washed with PBS. Sections were then blocked with a solution of PBS containing 1 droplet of normal horse serum according to the manufacturer's protocol (Vectastain ABC kit; Vector Laboratories) for 1 h at RT. Tissue sections were incubated with primary antibodies for detection of N protein (1/1,000; ascites fluid of the 4-E11.3 hybridoma) and activated astrocytes (1/1,000; rabbit anti-GFAP; Dako) overnight at 4°C. Tissue sections were washed with PBS three times and then incubated with secondary biotinylated antibody against mouse immunoglobulin G before being revealed with a Vectastain ABC kit.

**Statistical analysis.** Statistical analysis was performed using SimStat or XLSTAT software. Data are represented as means ± standard deviations (SD). For experiments on mice, statistical significance for survival curves was analyzed using a Kaplan-Meier test followed by a log-rank posttest (Mantel-Cox), and weight variation was analyzed with Kruskal-Wallis test followed by Tukey's *post hoc* test. For cell experiments, statistical analyses were conducted by Student *t* test or one-way analysis of variance (ANOVA) followed by Tukey's *post hoc* test.

## ACKNOWLEDGMENTS

We thank Jessie Tremblay for excellent technical assistance with confocal microscopy and Mathieu Dubé for helpful discussions.

This work was supported by grant no. MT-9203 from the CIHR's Institute of Infection and Immunity (III) to P.J.T., who is the holder of the Tier-1 (Senior) Canada Research Chair in Neuroimmunovirology award. M.M.-P. acknowledges a doctoral studentship from the Fonds de Recherche Québec–Santé, and A.L.C. acknowledges a doctoral studentship from the Fondation Universitaire Armand-Frappier de l'INRS. The funders had no role in study design, data collection and interpretation, or the decision to submit the work for publication.

## REFERENCES


1. Vabret A, Dina J, Brison E, Brouard J, Freymuth F. 2009. Human coronaviruses. Pathol Biol (Paris) 57:149–160. https://doi.org/10.1016/j.patbio.2008.02.018.
2. Forgie S, Marrie TJ. 2009. Healthcare-associated atypical pneumonia. Semin Respir Crit Care Med 30:67–85. https://doi.org/10.1055/s-0028-1119811.
3. Riski H, Hovi T. 1980. Coronavirus infections of man associated with diseases other than the common cold. J Med Virol 6:259–265. https://doi.org/10.1002/jmv.1890060309.
4. Yeh EA, Collins A, Cohen ME, Duffner PK, Faden H. 2004. Detection of coronavirus in the central nervous system of a child with acute disseminated encephalomyelitis. Pediatrics 113:e73259–e76. https://doi.org/10.1542/peds.113.1.e73.
5. McGavern DB, Kang SS. 2011. Illuminating viral infections in the nervous system. Nat Rev Immunol 11:318–329. https://doi.org/10.1038/nri2971.
6. Arabi YM, Harthi A, Hussein J, Bouchama A, Johani S, Hajeer AH, Saeed BT, Wahbi A, Saedy A, Al Dabbagh T, Okaili R, Sadat M, Balkhy H. 2015. Severe neurologic syndrome associated with Middle East respiratory syndrome corona virus (MERS-CoV). Infection 43:495–501. https://doi.org/10.1007/s15010-015-0720-y.
7. Morfopoulou S, Brown JR, Davies EG, Anderson G, Virasami A, Qasim W, Chong WK, Hubank M, Plagnol V, Desforges M, Jacques TS, Talbot PJ, Breuer J. 2016. Human coronavirus OC43 associated with fatal encephalitis. N Engl J Med 375:497–498. https://doi.org/10.1056/NEJMc1509458.
8. Buchmeier MJ, Dalziel RG, Koolen MJ, Lampert PW. 1987. Molecular determinants of CNS virulence of MHV-4. Adv Exp Med Biol 218:287–295. https://doi.org/10.1007/978-1-4684-1280-2_38.
9. Hosking MP, Lane TE. 2010. The pathogenesis of murine coronavirus infection of the central nervous system. Crit Rev Immunol 30:119–130. https://doi.org/10.1615/CritRevImmunol.v30.i2.20.
10. Jacomy H, Talbot PJ. 2003. Vacuolating encephalitis in mice infected by human coronavirus OC43. Virology 315:20–33. https://doi.org/10.1016/S0042-6822(03)00323-4.
11. Jacomy H, Fragoso G, Almazan G, Mushynski WE, Talbot PJ. 2006. Human coronavirus OC43 infection induces chronic encephalitis leading to disabilities in BALB/C mice. Virology 349:335–346. https://doi.org/10.1016/j.virol.2006.01.049.
12. Arbour N, Day R, Newcombe J, Talbot PJ. 2000. Neuroinvasion by human respiratory coronaviruses. J Virol 74:8913–8921. https://doi.org/10.1128/JVI.74.19.8913-8921.2000.
13. Favreau DJ, Desforges M, St-Jean JR, Talbot PJ. 2009. A human coronavirus OC43 variant harboring persistence-associated mutations in the S glycoprotein differentially induces the unfolded protein response in human neurons as compared to wild-type virus. Virology 395:255–267. https://doi.org/10.1016/j.virol.2009.09.026.
14. Favreau DJ, Meessen-Pinard M, Desforges M, Talbot PJ. 2012. Human coronavirus-induced neuronal programmed cell death is cyclophilin D dependent and potentially caspase dispensable. J Virol 86:81–93. https://doi.org/10.1128/JVI.06062-11.
15. Brison E, Jacomy H, Desforges M, Talbot PJ. 2011. Glutamate excitotoxicity is involved in the induction of paralysis in mice after infection by a human coronavirus with a single point mutation in its spike protein. J Virol 85:12464–12473. https://doi.org/10.1128/JVI.05576-11.
16. Brison E, Jacomy H, Desforges M, Talbot PJ. 2014. Novel treatment with neuroprotective and antiviral properties against a neuroinvasive human respiratory virus. J Virol 88:1548–1563. https://doi.org/10.1128/JVI.02972-13.
17. Jacomy H, St-Jean JR, Brison E, Marceau G, Desforges M, Talbot PJ. 2010. Mutations in the spike glycoprotein of human coronavirus OC43 modulate disease in BALB/c mice from encephalitis to flaccid paralysis and demyelination. J Neurovirol 16:279–293. https://doi.org/10.3109/13550284.2010.497806.
18. Linkermann A, Stockwell BR, Krautwald S, Anders HJ. 2014. Regulated cell death and inflammation: an auto-amplification loop causes organ failure. Nat Rev Immunol 14:759–767. https://doi.org/10.1038/nri3743.
19. Upton JW, Chan FK. 2014. Staying alive: cell death in antiviral immunity. Mol Cell 54:273–280. https://doi.org/10.1016/j.molcel.2014.01.027.
20. Galluzzi L, Brenner C, Morselli E, Touat Z, Kroemer G. 2008. Viral control of mitochondrial apoptosis. PLoS Pathog 4:e1000018. https://doi.org/10.1371/journal.ppat.1000018.
21. Galluzzi L, Vitale I, Abrams JM, Alnemri ES, Baehrecke EH, Blagosklonny MV, Dawson TM, Dawson VL, El-Deiry WS, Fulda S, Gottlieb E, Green DR, Hengartner MO, Kepp O, Knight RA, Kumar S, Lipton SA, Lu X, Madeo F, Malorni W, Mehlen P, Nunez G, Peter ME, Piacentini M, Rubinsztein DC, Shi Y, Simon HU, Vandenabeele P, White E, Yuan J, Zhivotovsky B, Melino G, Kroemer G. 2012. Molecular definitions of cell death subroutines: recommendations of the Nomenclature Committee on Cell Death 2012. Cell Death Differ 19:107–120. https://doi.org/10.1038/cdd.2011.96.
22. Wajant H, Pfizenmaier K, Scheurich P. 2003. Tumor necrosis factor signaling. Cell Death Differ 10:45–65. https://doi.org/10.1038/sj.cdd.4401189.
23. Seol DW, Li J, Seol MH, Park SY, Talanian RV, Billiar TR. 2001. Signaling events triggered by tumor necrosis factor-related apoptosis-inducing ligand (TRAIL): caspase-8 is required for TRAIL-induced apoptosis. Cancer Res 61:1138–1143.
24. Lettau M, Paulsen M, Schmidt H, Janssen O. 2011. Insights into the molecular regulation of FasL (CD178) biology. Eur J Cell Biol 90:456–466. https://doi.org/10.1016/j.ejcb.2010.10.006.
25. Feoktistova M, Geserick P, Panayotova-Dimitrova D, Leverkus M. 2012. Pick your poison: the Ripoptosome, a cell death platform regulating apoptosis and necroptosis. Cell Cycle 11:460–467. https://doi.org/10.4161/cc.11.3.19060.
26. Meylan E, Tschopp J. 2005. The RIP kinases: crucial integrators of cellular stress. Trends Biochem Sci 30:151–159. https://doi.org/10.1016/j.tibs.2005.01.003.
27. Dunai Z, Bauer PI, Mihalik R. 2011. Necroptosis: biochemical, physiological and pathological aspects. Pathol Oncol Res 17:791–800. https://doi.org/10.1007/s12253-011-9433-4.
28. Christofferson DE, Li Y, Hitomi J, Zhou W, Upperman C, Zhu H, Gerber SA, Gygi S, Yuan J. 2012. A novel role for RIP1 kinase in mediating TNFalpha production. Cell Death Dis 3:e320. https://doi.org/10.1038/cddis.2012.64.
29. Cho YS, Challa S, Moquin D, Genga R, Ray TD, Guildford M, Chan FK. 2009. Phosphorylation-driven assembly of the RIP1-RIP3 complex regulates programmed necrosis and virus-induced inflammation. Cell 137:1112–1123. https://doi.org/10.1016/j.cell.2009.05.037.
30. Zhang YY, Liu H. 2013. Connections between various trigger factors and the RIP1/RIP3 signaling pathway involved in necroptosis. Asian Pac J Cancer Prev 14:7069–7074. https://doi.org/10.7314/APJCP.2013.14.12.7069.
31. Baines CP. 2010. Role of the mitochondrion in programmed necrosis. Front Physiol 1:156.
32. Cai Z, Jitkaew S, Zhao J, Chiang HC, Choksi S, Liu J, Ward Y, Wu LG, Liu ZG. 2014. Plasma membrane translocation of trimerized MLKL protein is required for TNF-induced necroptosis. Nat Cell Biol 16:55–65.
33. Chen X, Li W, Ren J, Huang D, He WT, Song Y, Yang C, Li W, Zheng X, Chen P, Han J. 2014. Translocation of mixed lineage kinase domain-like protein to plasma membrane leads to necrotic cell death. Cell Res 24:105–121. https://doi.org/10.1038/cr.2013.171.
34. Le Coupanec A, Desforges M, Meessen-Pinard M, Dube M, Day R, Seidah NG, Talbot PJ. 2015. Cleavage of a neuroinvasive human respiratory virus spike glycoprotein by proprotein convertases modulates neurovirulence and virus spread within the central nervous system. PLoS Pathog 11:e1005261. https://doi.org/10.1371/journal.ppat.1005261.
35. Miyashita T, Krajewski S, Krajewska M, Wang HG, Lin HK, Liebermann DA, Hoffman B, Reed JC. 1994. Tumor suppressor p53 is a regulator of bcl-2 and bax gene expression in vitro and in vivo. Oncogene 9:1799–1805.
36. Miyashita T, Reed JC. 1995. Tumor suppressor p53 is a direct transcriptional activator of the human bax gene. Cell 80:293–299. https://doi.org/10.1016/0092-8674(95)90412-3.
37. Sharif-Askari E, Nakhaei P, Oliere S, Tumilasci V, Hernandez E, Wilkinson P, Lin R, Bell J, Hiscott J. 2007. Bax-dependent mitochondrial membrane permeabilization enhances IRF3-mediated innate immune response during VSV infection. Virology 365:20–33. https://doi.org/10.1016/j.virol.2007.03.011.
38. Xu W, Jing L, Wang Q, Lin CC, Chen X, Diao J, Liu Y, Sun X. 2015. Bax-PGAM5L-Drp1 complex is required for intrinsic apoptosis execution. Oncotarget 6:30017–30034. https://doi.org/10.18632/oncotarget.5013.
39. Vanlangenakker N, Vanden Berghe T, Vandenabeele P. 2012. Many stimuli pull the necrotic trigger, an overview. Cell Death Differ 19:75–86. https://doi.org/10.1038/cdd.2011.164.
40. Degterev A, Huang Z, Boyce M, Li Y, Jagtap P, Mizushima N, Cuny GD, Mitchison TJ, Moskowitz MA, Yuan J. 2005. Chemical inhibitor of nonapoptotic cell death with therapeutic potential for ischemic brain injury. Nat Chem Biol 1:112–119. https://doi.org/10.1038/nchembio711.
41. King MD, Whitaker-Lea WA, Campbell JM, Alleyne CH, Jr, Dhandapani KM. 2014. Necrostatin-1 reduces neurovascular injury after intracerebral hemorrhage. Int J Cell Biol 2014:495817.

42. Upton JW, Kaiser WJ, Mocarski ES. 2012. DAI/ZBP1/DLM-1 complexes with RIP3 to mediate virus-induced programmed necrosis that is targeted by murine cytomegalovirus vIRA. Cell Host Microbe 11:290–297. https://doi.org/10.1016/j.chom.2012.01.016.
43. Mack C, Sickmann A, Lembo D, Brune W. 2008. Inhibition of proinflammatory and innate immune signaling pathways by a cytomegalovirus RIP1-interacting protein. Proc Natl Acad Sci U S A 105:3094–3099. https://doi.org/10.1073/pnas.0800168105.
44. Chien H, Dix RD. 2012. Evidence for multiple cell death pathways during development of experimental cytomegalovirus retinitis in mice with retrovirus-induced immunosuppression: apoptosis, necroptosis, and pyroptosis. J Virol 86:10961–10978. https://doi.org/10.1128/JVI.01275-12.
45. Dondelinger Y, Declercq W, Montessuit S, Roelandt R, Goncalves A, Bruggeman I, Hulpiau P, Weber K, Sehon CA, Marquis RW, Bertin J, Gough PJ, Savvides S, Martinou JC, Bertrand MJ, Vandenabeele P. 2014. MLKL compromises plasma membrane integrity by binding to phosphatidylinositol phosphates. Cell Rep 7:971–981. https://doi.org/10.1016/j.celrep.2014.04.026.
46. Xu J, Ikezu T. 2009. The comorbidity of HIV-associated neurocognitive disorders and Alzheimer's disease: a foreseeable medical challenge in post-HAART era. J Neuroimmune Pharmacol 4:200–212. https://doi.org/10.1007/s11481-008-9136-0.
47. Brask J, Chauhan A, Hill RH, Ljunggren HG, Kristensson K. 2005. Effects on synaptic activity in cultured hippocampal neurons by influenza A viral proteins. J Neurovirol 11:395–402. https://doi.org/10.1080/13550280500186916.
48. Kavouras JH, Prandovszky E, Valyi-Nagy K, Kovacs SK, Tiwari V, Kovacs M, Shukla D, Valyi-Nagy T. 2007. Herpes simplex virus type 1 infection induces oxidative stress and the release of bioactive lipid peroxidation by-products in mouse P19N neural cell cultures. J Neurovirol 13:416–425. https://doi.org/10.1080/13550280701460573.
49. Soto C. 2003. Unfolding the role of protein misfolding in neurodegenerative diseases. Nat Rev Neurosci 4:49–60. https://doi.org/10.1038/nrn1007.
50. Butterfield DA, Reed T, Newman SF, Sultana R. 2007. Roles of amyloid beta-peptide-associated oxidative stress and brain protein modifications in the pathogenesis of Alzheimer's disease and mild cognitive impairment. Free Radic Biol Med 43:658–677. https://doi.org/10.1016/j.freeradbiomed.2007.05.037.
51. Mattson MP. 2003. Excitotoxic and excitoprotective mechanisms: abundant targets for the prevention and treatment of neurodegenerative disorders. Neuromol Med 3:65–94. https://doi.org/10.1385/NMM:3:2:65.
52. Schondorf DC, Aureli M, McAllister FE, Hindley CJ, Mayer F, Schmid B, Sardi SP, Valsecchi M, Hoffmann S, Schwarz LK, Hedrich U, Berg D, Shihabuddin LS, Hu J, Pruszak J, Gygi SP, Sonnino S, Gasser T, Deleidi M. 2014. iPSC-derived neurons from GBA1-associated Parkinson's disease patients show autophagic defects and impaired calcium homeostasis. Nat Commun 5:4028.
53. Das Sarma J, Kenyon LC, Hingley ST, Shindler KS. 2009. Mechanisms of primary axonal damage in a viral model of multiple sclerosis. J Neurosci 29:10272–10280. https://doi.org/10.1523/JNEUROSCI.1975-09.2009.
54. Zambrano A, Solis L, Salvadores N, Cortes M, Lerchundi R, Otth C. 2008. Neuronal cytoskeletal dynamic modification and neurodegeneration induced by infection with herpes simplex virus type 1. J Alzheimers Dis 14:259–269.
55. Leyssen P, Paeshuyse J, Charlier N, Van Lommel A, Drosten C, De Clercq E, Neyts J. 2003. Impact of direct virus-induced neuronal dysfunction and immunological damage on the progression of flavivirus (Modoc) encephalitis in a murine model. J Neurovirol 9:69–78. https://doi.org/10.1080/13550280390173319.
56. Kaczmarek A, Vandenabeele P, Krysko DV. 2013. Necroptosis: the release of damage-associated molecular patterns and its physiological relevance. Immunity 38:209–223. https://doi.org/10.1016/j.immuni.2013.02.003.
57. Pasparakis M, Vandenabeele P. 2015. Necroptosis and its role in inflammation. Nature 517:311–320. https://doi.org/10.1038/nature14191.
58. Li Y, Fu L, Gonzales DM, Lavi E. 2004. Coronavirus neurovirulence correlates with the ability of the virus to induce proinflammatory cytokine signals from astrocytes and microglia. J Virol 78:3398–3406. https://doi.org/10.1128/JVI.78.7.3398-3406.2004.
59. Liu Y, Pu Y, Zhang X. 2006. Role of the mitochondrial signaling pathway in murine coronavirus-induced oligodendrocyte apoptosis. J Virol 80:395–403. https://doi.org/10.1128/JVI.80.1.395-403.2006.
60. Liu Y, Zhang X. 2007. Murine coronavirus-induced oligodendrocyte apoptosis is mediated through the activation of the Fas signaling pathway. Virology 360:364–375. https://doi.org/10.1016/j.virol.2006.10.044.
61. Parquet MC, Kumatori A, Hasebe F, Morita K, Igarashi A. 2001. West Nile virus-induced bax-dependent apoptosis. FEBS Lett 500:17–24. https://doi.org/10.1016/S0014-5793(01)02573-X.
62. Deng L, Adachi T, Kitayama K, Bungyoku Y, Kitazawa S, Ishido S, Shoji I, Hotta H. 2008. Hepatitis C virus infection induces apoptosis through a Bax-triggered, mitochondrion-mediated, caspase 3-dependent pathway. J Virol 82:10375–10385. https://doi.org/10.1128/JVI.00395-08.
63. Castedo M, Ferri KF, Blanco J, Roumier T, Larochette N, Barretina J, Amendola A, Nardacci R, Metivier D, Este JA, Piacentini M, Kroemer G. 2001. Human immunodeficiency virus 1 envelope glycoprotein complex-induced apoptosis involves mammalian target of rapamycin/FKBP12-rapamycin-associated protein-mediated p53 phosphorylation. J Exp Med 194:1097–1110. https://doi.org/10.1084/jem.194.8.1097.
64. Lytvyn DIB, Ya B, Desforges M, Meessen-Pinard M, Talbot PJ, Sabater B, Martin M. 2016. Modulating regulated cell death: the virus way to influence cell fate, survive and persist. *In* Rice J (ed), Programmed cell death in plants and animals. Nova Science Publishers, New York, NY.
65. Poncet D, Pauleau AL, Szabadkai G, Vozza A, Scholz SR, Le Bras M, Briere JJ, Jalil A, Le Moigne R, Brenner C, Hahn G, Wittig I, Schagger H, Lemaire C, Bianchi K, Souquere S, Pierron G, Rustin P, Goldmacher VS, Rizzuto R, Palmieri F, Kroemer G. 2006. Cytopathic effects of the cytomegalovirus-encoded apoptosis inhibitory protein vMIA. J Cell Biol 174:985–996. https://doi.org/10.1083/jcb.200604069.
66. Su J, Wang G, Barrett JW, Irvine TS, Gao X, McFadden G. 2006. Myxoma virus M11L blocks apoptosis through inhibition of conformational activation of Bax at the mitochondria. J Virol 80:1140–1151. https://doi.org/10.1128/JVI.80.3.1140-1151.2006.
67. Cooray S, Bahar MW, Abrescia NG, McVey CE, Bartlett NW, Chen RA, Stuart DI, Grimes JM, Smith GL. 2007. Functional and structural studies of the vaccinia virus virulence factor N1 reveal a Bcl-2-like anti-apoptotic protein. J Gen Virol 88:1656–1666. https://doi.org/10.1099/vir.0.82772-0.
68. Marshall WL, Yim C, Gustafson E, Graf T, Sage DR, Hanify K, Williams L, Fingeroth J, Finberg RW. 1999. Epstein-Barr virus encodes a novel homolog of the bcl-2 oncogene that inhibits apoptosis and associates with Bax and Bak. J Virol 73:5181–5185.
69. D'Alessio M, De Nicola M, Coppola S, Gualandi G, Pugliese L, Cerella C, Cristofanon S, Civitareale P, Ciriolo MR, Bergamaschi A, Magrini A, Ghibelli L. 2005. Oxidative Bax dimerization promotes its translocation to mitochondria independently of apoptosis. FASEB J 19:1504–1506.
70. Garofalo RP, Kolli D, Casola A. 2013. Respiratory syncytial virus infection: mechanisms of redox control and novel therapeutic opportunities. Antioxid Redox Signal 18:186–217. https://doi.org/10.1089/ars.2011.4307.
71. Kumar S, Misra UK, Kalita J, Khanna VK, Khan MY. 2009. Imbalance in oxidant/antioxidant system in different brain regions of rat after the infection of Japanese encephalitis virus. Neurochem Int 55:648–654. https://doi.org/10.1016/j.neuint.2009.06.008.
72. Nakamura H, Masutani H, Yodoi J. 2002. Redox imbalance and its control in HIV infection. Antioxid Redox Signal 4:455–464. https://doi.org/10.1089/15230860260196245.
73. Han J, Zhong CQ, Zhang DW. 2011. Programmed necrosis: backup to and competitor with apoptosis in the immune system. Nat Immunol 12:1143–1149. https://doi.org/10.1038/ni.2159.
74. Re DB, Le Verche V, Yu C, Amoroso MW, Politi KA, Phani S, Ikiz B, Hoffmann L, Koolen M, Nagata T, Papadimitriou D, Nagy P, Mitsumoto H, Kariya S, Wichterle H, Henderson CE, Przedborski S. 2014. Necroptosis drives motor neuron death in models of both sporadic and familial ALS. Neuron 81:1001–1008. https://doi.org/10.1016/j.neuron.2014.01.011.
75. Zhu S, Zhang Y, Bai G, Li H. 2011. Necrostatin-1 ameliorates symptoms in R6/2 transgenic mouse model of Huntington's disease. Cell Death Dis 2:e115. https://doi.org/10.1038/cddis.2010.94.
76. Ofengeim D, Ito Y, Najafov A, Zhang YY, Shan B, DeWitt JP, Ye JY, Zhang XM, Chang AS, Vakifahmetoglu-Norberg H, Geng JF, Py B, Zhou W, Amin P, Lima JB, Qi CT, Yu Q, Trapp B, Yuan JY. 2015. Activation of necroptosis in multiple sclerosis. Cell Rep 10:1836–1849. https://doi.org/10.1016/j.celrep.2015.02.051.
77. Askalan R, Gabarin N, Armstrong EA, Fang Liu Y, Couchman D, Yager JY. 2015. Mechanisms of neurodegeneration after severe hypoxic-ischemic injury in the neonatal rat brain. Brain Res 1629:94–103. https://doi.org/10.1016/j.brainres.2015.10.020.
78. Jouan-Lanhouet S, Riquet F, Duprez L, Vanden Berghe T, Takahashi N, Vandenabeele P. 2014. Necroptosis, in vivo detection in experimental

disease models. Semin Cell Dev Biol 35:2–13. https://doi.org/10.1016/j.semcdb.2014.08.010.
79. Zhou W, Yuan J. 2014. Necroptosis in health and diseases. Semin Cell Dev Biol 35:14–23. https://doi.org/10.1016/j.semcdb.2014.07.013.
80. Pan T, Wu S, He X, Luo H, Zhang Y, Fan M, Geng G, Ruiz VC, Zhang J, Mills L, Bai C, Zhang H. 2014. Necroptosis takes place in human immunodeficiency virus type-1 (HIV-1)-infected CD4+ T lymphocytes. PLoS One 9:e93944. https://doi.org/10.1371/journal.pone.0093944.
81. Berger AK, Danthi P. 2013. Reovirus activates a caspase-independent cell death pathway. mBio 4:e00178-13.
82. Nogusa S, Thapa RJ, Dillon CP, Liedmann S, Oguin TH, III, Ingram JP, Rodriguez DA, Kosoff R, Sharma S, Sturm O, Verbist K, Gough PJ, Bertin J, Hartmann BM, Sealfon SC, Kaiser WJ, Mocarski ES, Lopez CB, Thomas PG, Oberst A, Green DR, Balachandran S. 2016. RIPK3 activates parallel pathways of MLKL-driven necroptosis and FADD-mediated apoptosis to protect against influenza A virus. Cell Host Microbe 20:13–24. https://doi.org/10.1016/j.chom.2016.05.011.
83. Wang X, Li Y, Liu S, Yu X, Li L, Shi C, He W, Li J, Xu L, Hu Z, Yu L, Yang Z, Chen Q, Ge L, Zhang Z, Zhou B, Jiang X, Chen S, He S. 2014. Direct activation of RIP3/MLKL-dependent necrosis by herpes simplex virus 1 (HSV-1) protein ICP6 triggers host antiviral defense. Proc Natl Acad Sci U S A 111:15438–15443. https://doi.org/10.1073/pnas.1412767111.
84. Guo H, Omoto S, Harris PA, Finger JN, Bertin J, Gough PJ, Kaiser WJ, Mocarski ES. 2015. Herpes simplex virus suppresses necroptosis in human cells. Cell Host Microbe 17:243–251. https://doi.org/10.1016/j.chom.2015.01.003.
85. Omoto S, Guo H, Talekar GR, Roback L, Kaiser WJ, Mocarski ES. 2015. Suppression of RIP3-dependent necroptosis by human cytomegalovirus. J Biol Chem 290:11635–11648. https://doi.org/10.1074/jbc.M115.646042.
86. Fan H, Tang HB, Kang J, Shan L, Song H, Zhu K, Wang J, Ju G, Wang YZ. 2015. Involvement of endoplasmic reticulum stress in the necroptosis of microglia/macrophages after spinal cord injury. Neuroscience 311:362–373. https://doi.org/10.1016/j.neuroscience.2015.10.049.
87. Saveljeva S, Mc Laughlin SL, Vandenabeele P, Samali A, Bertrand MJ. 2015. Endoplasmic reticulum stress induces ligand-independent TNFR1-mediated necroptosis in L929 cells. Cell Death Dis 6:e1587. https://doi.org/10.1038/cddis.2014.548.
88. He S, Wang L, Miao L, Wang T, Du F, Zhao L, Wang X. 2009. Receptor interacting protein kinase-3 determines cellular necrotic response to TNF-alpha. Cell 137:1100–1111. https://doi.org/10.1016/j.cell.2009.05.021.
89. Nakagawa T, Shimizu S, Watanabe T, Yamaguchi O, Otsu K, Yamagata H, Inohara H, Kubo T, Tsujimoto Y. 2005. Cyclophilin D-dependent mitochondrial permeability transition regulates some necrotic but not apoptotic cell death. Nature 434:652–658. https://doi.org/10.1038/nature03317.
90. Hill DP, Robertson KA. 1998. Differentiation of LA-N-5 neuroblastoma cells into cholinergic neurons: methods for differentiation, immunohistochemistry and reporter gene introduction. Brain Res Brain Res Protoc 2:183–190. https://doi.org/10.1016/S1385-299X(97)00041-X.
91. St-Jean JR, Desforges M, Almazan F, Jacomy H, Enjuanes L, Talbot PJ. 2006. Recovery of a neurovirulent human coronavirus OC43 from an infectious cDNA clone. J Virol 80:3670–3674. https://doi.org/10.1128/JVI.80.7.3670-3674.2006.
92. Lambert F, Jacomy H, Marceau G, Talbot PJ. 2008. Titration of human coronaviruses, HcoV-229E and HCoV-OC43, by an indirect immunoperoxidase assay. Methods Mol Biol 454:93–102. https://doi.org/10.1007/978-1-59745-181-9_8.